Engineering 7 (2021) 304–325

Contents lists available at ScienceDirect

Engineering

journal homepage: www.elsevier.com/locate/eng

Research
Green Chemical Engineering—Review

Process Intensification in Pneumatically Agitated Slurry Reactors

Shujun Geng [a,b], Zai-Sha Mao [c], Qingshan Huang [a,b,*], Chao Yang [a,b,c,*]

[a] Key Laboratory of Biofuels, Qingdao Institute of Bioenergy and Bioprocess Technology, Chinese Academy of Sciences, Qingdao 266101, China
[b] Dalian National Laboratory for Clean Energy, Dalian Institute of Chemical Physics, Chinese Academy of Sciences, Dalian 116023, China
[c] Key Laboratory of Green Process and Engineering, Institute of Process Engineering, Chinese Academy of Sciences, Beijing 100190, China

ARTICLE INFO

Article history:
Received 28 January 2019
Revised 24 August 2019
Accepted 17 December 2019
Available online 11 March 2021

Keywords:
Slurry reactors
Pneumatic agitation
Bubble column
Airlift loop reactor
Process intensification
Solid particles

ABSTRACT

Pneumatically agitated slurry reactors, including bubble column reactors and airlift loop reactors (ALRs), are important gas–liquid–solid multiphase reactors. These reactors have been widely applied in many processes, especially in the biological fermentation and energy chemical industry, due to their low shear stress, good mixing, perfect mass-/heat-transfer properties, and relatively low costs. To further improve the performance of slurry reactors (i.e., mixing and mass/heat transfer) and to satisfy industrial requirements (e.g., temperature control, reduction of back-mixing, and product separation), the process intensification of slurry reactors is essential. This article starts by reviewing the latest advancements in the intensification of mixing and mass/heat transfer in these two types of reactors. It then summarizes process-intensification methods for mixing and separation that allow continuous production in these slurry reactors. Process-intensification technology that integrates directional flow in an ALR with simple solid–liquid separation in a hydrocyclone is recommended for its high efficiency and low costs. This article also systematically addresses vital considerations and challenges, including flow regime discrimination, gas spargers, solid particle effects, and other concerns in slurry reactors. It introduces the progress of numerical simulation using computational fluid dynamics (CFD) for the rational design of slurry reactors and discusses difficulties in modeling. Finally, it presents conclusions and perspectives on the design of industrial slurry reactors.

1. Introduction

Pneumatically agitated slurry reactors are characterized by buoyancy-driven flow with an acceptable energy input for mixing but without moving parts. The most common examples of this type of reactors are the bubble column and the airlift loop reactor (ALR). These reactors have been widely used in processes for gas–liquid and gas–liquid–solid multiphase reactions, such as biological fermentation [1], wastewater treatment [2], the mass cultivation of photosynthetic organisms [3,4], and the energy chemical industry [5] due to their simple construction, excellent mass- and heat-transfer properties, and relatively low energy consumption [6]. In addition to these advantages, ALRs possess low and uniform shear stress [7,8], which is necessary for biological reactions [7,9]. There are two types of ALR: the internal airlift loop reactor (IALR) and the external airlift loop reactor (EALR). The hydrodynamics in ALRs (e.g., gas holdup, solid holdup, liquid velocity, bubble-size distribution, flow regime, mixing time, residence time distribution), mass-transfer properties, heat-transfer coefficient, and reaction rate, which represent the operating performance, have been thoroughly investigated with varying structural parameters (e.g., reactor height [10], downcomer-to-riser cross-sectional area ratio [11], and gas distributor [12]) and operating conditions (e.g., temperature, pressure [5], superficial gas velocity [13], and solid concentration [14]). Based on the experimental data and energy-balance equations, various theoretical and empirical correlations have been deduced to predict the hydrodynamics and transport properties in these slurry reactors [15,16]. It should be noted that the proposed relations have some restrictions on operating conditions and structural parameters due to limited mathematical statistics or the simplification of balance equations.

Along with numerous investigations in traditional pneumatically agitated reactors, various studies have focused on the design and optimization of novel slurry reactors for process intensification for different industrial purposes. Specifically, internal tubes can be installed for heat exchange in order to maintain reactors at the

* Corresponding authors.
E-mail addresses: qshuang@ipe.ac.cn (Q. Huang), chaoyang@ipe.ac.cn (C. Yang).

https://doi.org/10.1016/j.eng.2021.03.002

desired temperature; baffles, static mixers, and mechanical internals can be equipped to enhance the overall mixing [17,18]; perforated plates can be used to reduce liquid back-mixing [19,20]. With the application of coated structured catalysts, no extra separation of liquid and solid catalysts is necessary [21]. Hydrodynamics, mass-transport properties, and mixing characteristics have been investigated in these novel pneumatically agitated reactors, and various empirical correlations have been proposed to predict and optimize their structures.

Great endeavors have been undertaken to improve the performance of slurry reactors and to meet the desired requirements for different industrial processes. For the Fischer–Tropsch synthesis, fixed-bed reactors, multitubular reactors, slurry reactors, and circulated fluidized-bed reactors have been commercialized [22]. Industrial gas–liquid–solid slurry reactors with internal cooling tubes, which are suitable for producing diesel and paraffin wax [23], are prospective slurry reactors due to their excellent mixing and mass-/heat-transfer properties. Suspended catalytic particle separation is one of the biggest challenges in slurry reactors, igniting the development of integral catalyst design (i.e., honeycombs, structured packings, or foams) and the integration of mixing and separation [24,25]. The slurry reactor design and concerns are similar to those of other gas-to-liquid processes, such as methanol synthesis and dimethyl ether synthesis [26]. Compared with conventional stirred tanks and bubble columns, the ALR has been verified to be an effective device for wastewater treatment due to its high adsorption efficiency and low shear stress to cells [27]. Furthermore, various techniques, such as biofilm, membrane, electrocoagulation, ultrasound, and photochemical methods, can be conveniently combined with ALRs, providing numerous alternatives for wastewater treatment and biological fermentation [28].

This article reviews intensification concepts and techniques for both gas–liquid and gas–liquid–solid flows in aerated reactors and presents related industrial processes. It also summarizes the relevant empirical and theoretical relationships of the hydrodynamics and transport properties in intensified slurry reactors. The article is organized as follows: Section 2 provides an overview of the intensification methods of mixing and mass/heat transfer in bubble columns and ALRs, including internals (i.e., internal tubes, perforated plates, baffles, static mixers, structuring or packed beds, and mechanical internals), vibrating excitement, and combination methods. It also describes and compares intensified methods and their influence on hydrodynamics and transport properties. In light of the challenges of separating solid catalyst particles from continuous liquid products, Section 3 outlines separation methods applied in slurry reactors, with a focus on settling (both gravitational and centrifugal), filtration, and composite methods. Section 4 then elaborates important design considerations and challenges for the industrial design of pneumatically agitated slurry reactors. With the rapid development of computational fluid dynamics (CFD), mathematical modeling has become an efficient method for the design, optimization, and scale-up of slurry reactors. It can also be considered as an intensification method for substantial improvement of the performance in pneumatically agitated slurry reactors. Thus, Section 5 focuses on CFD modeling. Finally, Section 6 provides conclusions and perspectives on pneumatically agitated slurry reactors.

2. Process intensification of mixing and mass/heat transfer

It is widely accepted that the vital feature in a bubble column reactor is the non-ideal flow pattern for each phase, which can significantly influence reactant conversion and selectivity [29]. However, directional flow for each phase is an outstanding advantage in the ALR [7]. Therefore, the technologies of process intensification should be diversified due to the nature of their flow.

2.1. Bubble columns

The bubble column has been widely applied in chemical, biochemical, and petrochemical processes, such as hydrogenation, fermentation, and Fischer–Tropsch synthesis, due to its simple construction, low energy cost, and good mass- and heat-transfer properties [19,30,31]. It has been reported that the bubble column reactor is now competitive with the traditional fixed-bed reactor for converting syngas into liquid fuels [32]. Most reactions conducted in a bubble column must be maintained within a suitable temperature range by the addition of internal heat-exchanging tubes. Moreover, the flow structure should be reasonably controlled to enlarge the gas–liquid interfacial area and reduce back-mixing in order to improve the gas–liquid mass transfer and reduce byproducts. Installing different types of internals and enforcing constant-frequency flow pulsation are two main approaches to intensify hydrodynamic interactions, mass-/heat-transfer properties, and reactant conversion and selectivity in bubble columns.

2.1.1. Intensification with internals

2.1.1.1. Internal tubes. Many of the chemical reactions occurring in a bubble column are highly exothermic, such as Fischer–Tropsch synthesis, methanol synthesis, and acetic acid production; thus, a bundle of heat-exchange tubes is necessary to maintain the desired reaction temperature and avoid local overheating [22,33]. In the 1990s, Sasol developed a slurry reactor with internally cooled tubes for Fischer–Tropsch synthesis, with a capacity of 2500 $bbl \cdot d^{-1}$ (1 bbl = 158.9873 L) [23]. For the methanol synthesis process, a bubble column with a diameter of 457.2 mm equipped with internal tubes was developed by Alternate Fuels Development Unit in La Porte, Texas, USA [19]. Fig. 1 [34] provides a schematic diagram of a bubble column equipped with internal tubes. It has been shown that the gas holdup and bubble passage frequency increase with the installation of internal tubes inside the column [34]. At the same time, the bubble chord length and bubble-rise velocity decrease due to the enhancement of bubble breakup, especially for dense internals with high occupation of the cross-sectional area [35,36]. The bundle of internal tubes is commonly arranged in a hexagonal or circular pattern (Fig. 1). Different kinds and sizes of internals can influence the hydrodynamics and transfer properties

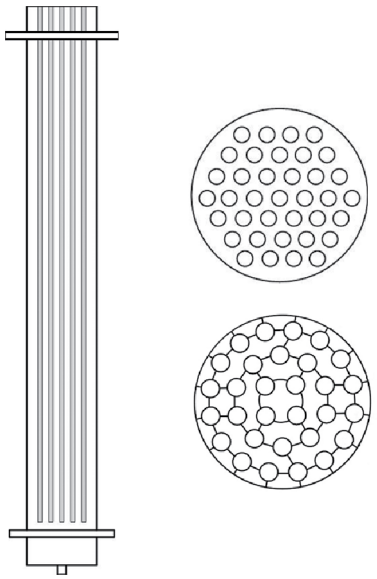

Fig. 1. Schematic diagram of a bubble column equipped with inner tubes. Reproduced from Ref. [34] with permission of American Chemical Society, ©2009.

in different ways and subsequently affect the reactant conversion and selectivity in bubble column reactors. Investigations on bubble columns equipped with different arrangements of internal tubes are summarized in Table 1 [20,34,35,37–44].

Kagumba and Al-Dahhan [35] investigated the hydrodynamics through four-point fiber optical probes in a bubble column equipped with a bundle of two different-diameter vertical tubes (i.e., 12.7 and 25.4 mm, respectively), with the same occupation of the cross-sectional area (25%). It was found that the local gas holdup at the column center was enhanced by up to 40% in the bubbly flow regime when the superficial gas velocity was 0.03 m·s^{-1}, and that the promotion of gas holdup was greater with 25.4 mm internals than with 12.7 mm internals in the bubble column. However, the gas holdup only attained an average increase of 2% for both the 25.4 and 12.7 mm tubes in the churn turbulent flow regime at a superficial gas velocity of 0.45 m·s^{-1}. Regarding the specific interfacial area and bubble passage frequency, it was observed that the values obtained when using 12.7 mm internals attained a higher increase than the values obtained when using 25.4 mm internals with a superficial gas velocity ranging from 0.03 to 0.45 m·s^{-1}. However, Sultan et al. [45] obtained different conclusions indicating that two different-sized internals had negligible influence on the local gas holdup in the bubbly flow regime, while a higher gas holdup was obtained with 25.4 mm internals in the region close to the wall in the turbulent regime when the superficial gas velocity was 0.45 m·s^{-1}. It was also demonstrated that the gas holdup showed a wavy radial distribution in a bubble column with internals, compared with a parabolic distribution in a

Table 1
Summary of investigations on bubble columns equipped with internals.

Internal type	Ref.	System	Dimension of column	Internal details	Operating conditions	Influences of internals
Internal tubes	Youssef and Al-Dahhan [34]	Air–water	D = 0.19 m, H = 2 m	Circular arranged, α = 5%; hexagonal arranged, α = 22%	U_g = 0.03–0.20 m·s^{-1}	U_g = 0.2 m·s^{-1} Overall ε_g: α = 5%, no significant improvement; α = 22%, –18% increase Local ε_g: α = 5%, 15.1% increase; α = 22%, 32.8% increase Interfacial area a: α = 5%, 19.4% increase; α = 22%, 70.7% increase
	Kagumba and Al-Dahhan [35]	Air–water	D = 0.14 m, H = 1.83 m	α = 25%, d_{tube} = 12.7 mm, 25.4 mm	U_g = 0.03–0.45 m·s^{-1}	U_g calculation based on free cross-sectional area, no significant enhancement of overall ε_g was achieved Based on total sectional area, for Local ε_g: U_g = 0.03 m·s^{-1}: d_{tube} = 12.7 mm, 22.7% increase; d_{tube} = 25.4 mm, 40.8% increase; U_g = 0.45 m·s^{-1}: no significant increase (–2%)
	Pradhan et al. [37]	Air–CMC	D = 0.102 m, H = 2.5 m	α = 1.4%–19.3%; straight tubes; helical coils	U_g = 0.014–0.193 m·s^{-1}	U_g = 0.041 m·s^{-1}, overall ε_g: straight tubes, α = 10.8%, 19.5% increase; helical coils, α = 3.9%, 48.4% increase
	Saxena et al. [38]	Air–water; air–water–glass	D = 0.305 m, H = 3.25 m	Sparsely arranged: N_{tube} = 5, α = 1.9%; hexagonal arranged: N_{tube} = 37, α = 14.3%; N_{tube} = 7, α = 2.7%	U_g = 0–0.24 m·s^{-1}, T = 293–363 K	Overall ε_g: T < 313.15 K, $\varepsilon_{g,N_{tube}=37} > \varepsilon_{g,N_{tube}=7} > \varepsilon_{g,N_{tube}=5}$ T > 313.15 K, $\varepsilon_{g,N_{tube}=7} > \varepsilon_{g,N_{tube}=37} > \varepsilon_{g,N_{tube}=5}$
Perforated plates	Fair et al. [39]	Air–water	D = 0.4572 m, 1.016 m; H = 3.25 m	N_b = 1–20, d_o = 3.175–7.925 mm, α = 9.5%–33.0%	U_g = 0.0152–0.1006 m·s^{-1}	Overall ε_g: static baffles, 40%–50% increase; moving baffles, 25%–30% further increase Heat transfer: 10%–15% increase
	Palaskar et al. [40]	Air–water	D = 0.062 m, H = 0.77 m; D = 0.2 m, H = 0.9 m	N_b = 4; α = 0.5%, 1.48%, 10.8%, 100%; d_o = 3.17 mm	U_g = 1.66 × 10^{-4}–2.00 × 10^{-3} m·s^{-1}, U_l = 3.75 × 10^{-4}–2.00 × 10^{-3} m·s^{-1}	Reduce liquid back-mixing, $\ln[D_{s,l}/(U_l H_l)] = D^{-0.2}\left\{0.023[\ln(FP)]^2 + 0.2658\ln(FP) - 0.816\right\}$ where a lumped flow parameter $FP = U_g\alpha/U_l$
	Dreher and Krishna [20]	Air–water	D = 0.1 m, H = 6 m; D = 0.15 m, H = 4 m; D = 0.38 m, H = 4 m	N_b = 1–2; d_o = 10 mm; α = 18.6%, 30.7%	U_g = 0.05–0.40 m·s^{-1}	Liquid circulation magnitude was reduced one order (–85%, α = 18.6%) compared to empty column Liquid circulation magnitude increased 118.8% from α of 18.6% to 30.7%
Static mixers	Rabha et al. [41]	Air–water	D = 0.08 m, H = 3.45 m	Helical static mixer; h = 0.08 m; θ = 180°; N_{mixer} = 3, 6, 9	U_g = 0.11–0.42 m·s^{-1}, U_l = 0.2–0.6 m·s^{-1}	U_g/U_l = 0.183, d_b decreased 42% U_g/U_l = 0.383, d_b decreased 19% U_g/U_l = 1.15, d_b increased 13%
	Gaspillo and Goto [42]	Gas–liquid–solid	D = 0.097 m, H = 0.37 m	Draft tube, Kenics mixer	U_g = 0.0015–0.0157 m·s^{-1}, ε_s = 0–10%	ε_s = 10%, $u_{g,min}$: draft tube only decreased 53.2%, draft tube and static mixer decreased 44.7%; k_La increased 20% with draft tube and static mixer
Structuring	Urseanu et al. [43]	Air–water	D = 0.1 m, 0.24 m	KATAPAK-S, θ = 45°	U_g = 0–0.65 m·s^{-1}	Based on free sectional area, overall gas holdup maintained same as empty column; liquid back-mixing reduced by one order of magnitude; $D_{s,l}$ = 0.081U_l
	Khamadieva and Böhm [44]	Air–CMC	4 cm × 4 cm × 80 cm	Sulzer-Mellapak, h = 4 cm, N = 2–5, plastic packing	U_g = 0.005–0.075 m·s^{-1}	Only for non-Newtonian fluid, liquid to wall mass transfer was enhanced $Sh = 0.146(ScGa)^{0.36}\varepsilon_g^{0.23}$

All the symbols in this table are defined in the Nomenclatures list at the end of this paper.
CMC: carboxy-methyl cellulose.

column without internals. In addition, the shape and steepness of the radial profile of the gas holdup had a relationship with the number of internal bundles and sizes, which was also reported by Al Mesfer et al. [46].

Pradhan et al. [37] investigated the influences of the volume fraction occupied by internal tubes on the overall gas holdup by varying the superficial gas velocity. When the volume fraction of the internals was increased from 1.4% to 19.3%, the gas holdup increased monotonously, regardless of whether straight tubes or helical coils were installed. Moreover, a higher gas holdup was obtained with helical coils than with straight tubes. To be specific, the gas holdup was increased by about 19.5% when the straight tubes occupied a volume fraction of 10.8%, compared with 48.4% enhancement when the helical coils occupied a volume fraction of 3.9%, for a superficial gas velocity of 0.41 $m{\cdot}s^{-1}$. Youssef and Al-Dahhan [34] also reported that the overall and local gas holdup and the interfacial area increased when the occupation of the cross-sectional area covered by internals was increased, especially at the center of the bubble column.

Saxena et al. [38] investigated the gas holdup of both air–water and air–water–glass systems in a bubble column equipped with five sparsely arranged tubes, and with seven tubes and 37 tubes with tightly hexagonal arrangements, occupying 1.9%, 2.7%, and 14.3% of the column cross-sectional area, respectively. Their results demonstrated that the overall gas holdup in the bubble column equipped with 37 tubes was notably higher than that in the columns with five and seven tubes, respectively, when the superficial gas velocity was above 0.1 $m{\cdot}s^{-1}$. However, when the superficial gas velocity was less than 0.1 $m{\cdot}s^{-1}$, the differences in gas holdup between columns with differently arranged tubes were obscure, and the column equipped with seven central tubes achieved the highest gas holdup at ambient temperature. It was also observed that the centrally arranged internal tubes were apt to increase the gas holdup due to the enhancement of bubble breakup in the center region. For a three-phase system, the gas holdup decreased with increasing particle size from 125 to 212 μm when the solid concentration was greater than 5%, with temperature varying from 298 to 353 K. In contrast, the variation tendency of the gas holdup versus the particle diameter was sensitive to temperature for dilute slurries (about 5 wt%). The gas holdup decreased with increasing particle diameter at ambient temperature, with no variation being observed above 323 K.

Based on the discussion above, the enhancement of hydrodynamics by internal tubes is related to their size, occupation area of the cross-section, arrangement, and operational conditions. In general, greater promotion of gas holdup is obtained with greater occupation of the cross-sectional area, and regular centrally arranged internal tubes are more beneficial for bubble breakup.

2.1.1.2. Perforated plates. Perforated plates are one of the most traditional internals used to intensify the hydrodynamics and mass/heat transfer in bubble columns [47]. As early as 1962, Fair et al. [39] investigated gas holdup and heat transfer in pilot-scale bubble columns with an air–water system. The bubble columns were 457.2 or 1016 mm in diameter and 3048 mm in height and were equipped with 1–20 static or moving perforated plates. The pore diameter of the perforated baffles varied from 3.175 to 7.925 mm; the opening area ranged from 9.5% to 33.0% of the cross-sectional area; the numbers of equipped baffles were 5, 10, 15, and 20, respectively. With the assembly of static plates, the gas holdup was increased by 40%–50% compared with that in an empty bubble column and further increased by 25%–30% caused by the moving perforated plates when the superficial gas velocity was changed from 1.524 to 10.06 $cm{\cdot}s^{-1}$. Analogously, heat transfer was promoted by 10%–15% as a result of both stationary and moving perforated plates. The enhancements of perforated plates in bubble columns are summarized in Table 1.

Intense liquid back-mixing is a distinct feature of the slurry bubble column reactor and may reduce the selectivity and conversion of reactant. It has been reported that the liquid axial dispersion can be regulated by sectioning a bubble column with perforated plates [48]. The extent of liquid back-mixing decreases with a decrease in pore diameter and in the free area percentage of the orifice plates [40]. This decrease has been ascribed to the uniform redistribution of the dispersed phase at each plate with the increase of gas flow resistance and minimization of the density gradient. Nevertheless, the new problem of choking has been found to occur much more easily with a low opening fraction and small pore diameter of sieve plates. Thus, the appropriate design of the number, pore diameter, and free area percentage of perforated plates is important to achieve the desired hydrodynamics and liquid dispersion characteristics [48]. The axial dispersion model is commonly employed to depict the residence time distribution of the liquid phase in bubble columns [49,50]. It was found that the axial dispersion coefficient was related to an exponential function of the superficial liquid velocity, with an exponent ranging from 0.234 to 0.85 [40] when the net liquid velocity relative to the rising bubbles was less than 10% of the bubble-rising velocity [51]. However, the liquid axial dispersion coefficient was independent of the superficial liquid velocity if the circulation velocity was ten times higher than the superficial liquid velocity [52]. Furthermore, the liquid axial dispersion coefficient was found to be dependent on an exponential function of the superficial gas velocity, with an exponent ranging from 0.12 to 0.33 [40,52]. Dreher and Krishna [20] studied the liquid residence time distribution using the axial dispersion model with the liquid exchange velocity for quantitative calculation. Their results showed that the liquid exchange velocity was independent of the column diameter, which was important for the scale-up of multi-stage bubble column reactors.

2.1.1.3. Static mixers. Static mixers have been widely applied to disperse the gas phase in liquid bulk in chemical and industrial processes due to their minimal space requirement and low equipment cost, and the fact that they do not require extra power supply [53]. The commercial Inliner mixer, produced by Lightnin Inc., has been applied in petrochemical industrial processes such as hydrocarbon refining [53]. With a static mixer inserted, the gas–liquid interfacial area in the column is increased, and the mass/heat transfer and chemical reactions are intensified. Fig. 2(a) [41] shows a schematic diagram of a bubble column equipped with static mixers, and Fig. 2(b) [53] depicts common types of static mixer. The rate of gas–liquid mass transfer was nearly double in bubble columns packed with Koch static mixers, compared with that in an unpacked bubble column, as investigated by Fan et al. [54] and Wang and Fan [55] with a liquid velocity ranging from 6.7 to 39.9 $cm{\cdot}s^{-1}$. These researchers also deduced a correlation of the volumetric mass-transfer coefficient (k_La), with V_l (where V_l is the liquid velocity) as an independent variable.

Gaspillo and Goto [42] studied the influence of a static mixer in a draft tube on the minimum gas velocity to suspend the solid particles and mass-transfer coefficient in both gas–liquid and gas–liquid–solid slurry bubble columns. It was demonstrated that the minimum gas velocity for slurry suspension decreased with the presence of a draft tube but slightly increased with the addition of a static mixer, which might be caused by the turbulent motion of solid particles in the static mixer. When a single-nozzle gas distributor was used, the gas–liquid mass-transfer coefficient increased by about 34% with the static mixer installed. Nevertheless, when an orifice ball distributor was applied to produce extremely fine bubbles, the gas–liquid mass-transfer coefficient decreased due to bubble coalescence caused by the static mixer. The rate of gas–liquid mass transfer increased by about 20% with the static mixer equipped in the draft tube, regardless of which kind of gas

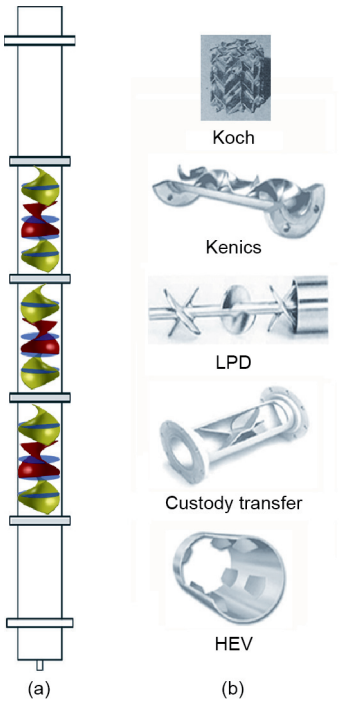

Fig. 2. (a) Schematic diagram of a bubble column equipped with static mixers; (b) common types of static mixer. LPD: low pressure drop; HEV: high efficiency vortex. (a) Reproduced from Ref. [41] with permission of Elsevier B.V., ©2014; (b) reproduced from Ref. [53] with permission of Institution of Chemical Engineers, ©2003.

distributor was adopted. Table 1 depicts the improvement in hydrodynamics and mass transfer.

Recently, Rabha et al. [41] evaluated the length of the helical mixer on the gas holdup, gas-phase flow structure, interfacial area, and bubble-size distribution using ultrafast electron beam X-ray tomography. Three, six, and nine helical static mixers that were 80 mm in diameter, 80 mm in length, and had a 180-degree rotation of the blade, were inserted in the column to investigate their impact. The liquid velocity and helical structure induced extra shear, forcing bubble breakup. At a low flow ratio (U_g/U_l), the bubble size distribution was notably narrowed, and large bubbles suddenly decreased in size after flowing through these static mixers. Compared with the bubble diameter at the same axial position before the mixers, the bubble Sauter diameter decreased by about 42% regardless of the number of static mixers, as displayed in Fig. 3(a). With an increase of superficial gas velocity, the quantitative reduction of the bubble Sauter diameter decreased and the number of large bubbles increased due to bubble coalescence during turbulent swirling motions, as shown in Fig. 3(b) [41]. Nonetheless, when the flow ratio was increased with a low liquid velocity, the large bubbles could not be clearly dispersed by the static mixers, resulting in a slight increase in the bubble Sauter diameter. Similarly, it was observed that the specific gas–liquid interfacial area varied with the mixer elements because the interfacial area was directly related to the bubble diameter and liquid circulation.

Thus, to realize process intensification in a slurry bubble column, the structure and scale of the static mixer elements should be appropriately designed while considering the gas distributor, other internals, and the operating conditions.

2.1.1.4. Structuring. Liquid–solid separation and reducing back-mixing are typical challenges in a pneumatically agitated slurry reactor because the separation process can increase the operating and capital costs, while back-mixing decreases the selectivity and conversion of reactant. Structuring the reactor by equipping regular internals has been identified as an efficient method to intensify the slurry bubble column reactor to avoid solid–liquid separation and to reduce back-mixing. On the one hand, catalysts are structured into monoliths or coated on regular internals in the reactor so that it is not necessary to separate solid catalyst particles from the liquid products. On the other hand, the exact shape and size of column internals are designed to guide the flow to reduce liquid back-mixing. Furthermore, the internal structure can be designed precisely according to catalytic, reaction kinetics, and heat-transfer characteristics, making scale-up much easier [21,56]. Structured packing has been successfully applied in industrial absorption and distillation processes and then applied in the chemical and petrochemical industries [57]. Meanwhile, a packed bed is suitable for acetic acid production due to its high surface-specific area [58].

Structured packing can be classified into four kinds: monoliths with parallel straight channels, corrugated sheets with open or closed flow structure, knitted wire packing, and open-celled foams [59]. High porosity, high surface area, and a low pressure drop are common and essential features of structured packing, in order to provide a sufficient specific surface area for heat and mass transfer and to restrict energy consumption. Structured packing has been proven to promote radial heat [21] and mass-transfer rates [60], thus increasing the reactant conversion and productivity [56]. Although the structured bubble column has been widely investigated, most relevant research has focused on the co-current tricked bed [59,61,62] rather than on the countercurrent bubble column.

Using open cross-flow structure (KATAPAK-S elements, supplied by Sulzer Chemtech) packing in two bubble column reactors with diameters of 0.1 and 0.24 m, respectively, Urseanu et al. [43] investigated the hydrodynamics and mixing characteristics in comparison with those in an empty bubble column. Fig. 4 [43,59] shows a schematic diagram of the experimental setup. The experimental results showed that the total gas holdup in the structured bubble column was almost the same as that in the empty bubble column at the same superficial gas velocity based on the free cross-sectional area. It could then be inferred that the existence of structured packing did not promote additional bubble coalescence and breakup. In regard to axial mixing characteristics, the axial dispersion factor—which was developed by Krishna et al. [49]—decreased by about one order of magnitude at a superficial gas velocity of up to 1.25 $m{\cdot}s^{-1}$ due to inhibition of the overall axial recirculation of the liquid phase. Moreover, axial dispersion could be fitted into a linear correlation with the liquid velocity for both the empty and structured bubble columns.

The gas holdup and liquid-to-wall mass transfer in structured and empty bubble columns were measured in a square sectional reactor, as described in Ref. [44]. The results showed that the gas holdup increased with an increase of the superficial gas velocity and liquid viscosity in the packed bubble column. Under the same operating conditions, the gas holdup in the structured column was higher than that in the empty column. Similar correlations of mass transfer were derived for the structured packing and empty column, regardless of whether Newtonian or non-Newtonian fluids were used. This result indicated that structured packing had a negligible influence on the liquid–wall mass transfer.

2.1.2. Intensification with vibrating excitement

Vibration exciters, such as pulsators, bellows, pistons, electric cams, and electromagnetic vibrators, can be installed at the bottom of the column to generate the necessary frequencies of vibration directly in the slurry within the reactor. Fig. 5 provides a schematic diagram of a common pulsing bubble column. The introduction of overall pulsations to the liquid in a bubble column has been substantially confirmed as an effective method for improving the gas–liquid mass- and heat-transfer properties [63,64]. Numerous

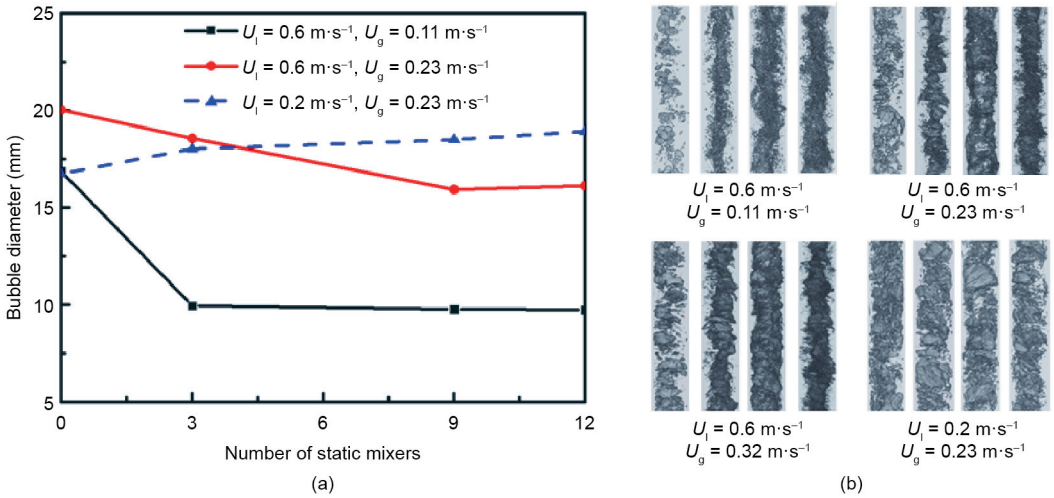

Fig. 3. Influence of static mixer length on bubble diameter (a) quantitatively and (b) qualitatively under different liquid and gas superficial velocities. Reproduced from Ref. [41] with permission of Elsevier B.V., ©2014.

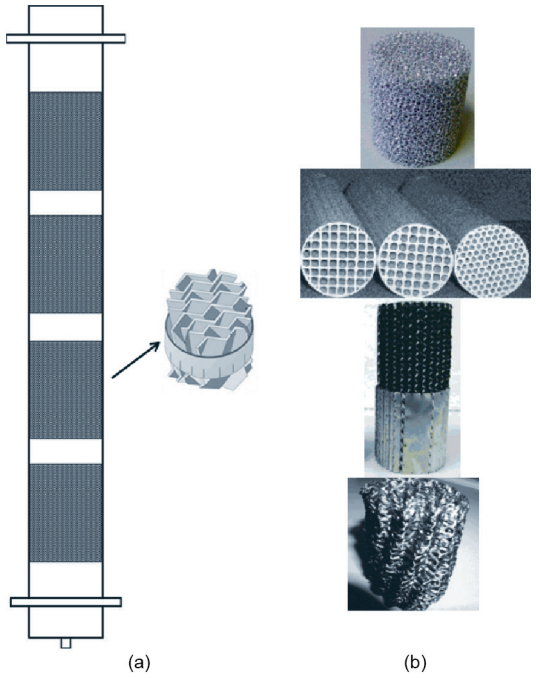

Fig. 4. (a) Schematic diagram of a structured bubble column including a packed element; (b) typical examples of cordierite monoliths. (a) Reproduced from Ref. [43] with permission of Elsevier Science B.V., ©2001; (b) reproduced from Ref. [59] with permission of American Chemical Society, ©2008.

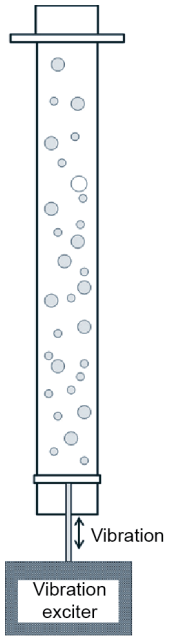

Fig. 5. Schematic diagram of a bubble column intensified by vibration.

studies have been conducted to explore the influence of oscillations on the hydrodynamics and mass-transfer properties, with the aim of revealing the relationships between the performance and operating conditions in a bubble column. Table 2 [64–73] summarizes relevant investigations and critical findings on intensification by vibration.

Ellenberger et al. [64–67] systematically investigated the bubble diameter, gas holdup, and mass-transfer characteristics in air–water and air–water–silica bubble columns subjected to low-frequency vibration (40–200 Hz). For a single-orifice gas distributor under a constant superficial gas velocity, the bubble diameter first decreased sharply with an increase in vibration frequency and amplitude, and then ultimately reached a relative plateau at a vibration frequency of around 100 Hz. Similar trends of bubble diameter versus vibration amplitude were observed; however, the inflection point varied with the superficial gas velocity. The bubble diameter was reduced by 40%–50% when the orifice gas velocity ranged from 0.2 to 3 m·s^{-1} with a pulsing frequency and amplitude of around 100 Hz and 1 mm, respectively. To analyze the mechanisms of bubble breakup in a pulsing bubble column, Knopf et al. [68,69] applied a high-speed camera to observe the bubble-formation process in a glass gas T-injector. The liquid phase was forced by a flexible piston at low frequencies (0–30 Hz) with a low amplitude. When the gas flow rate was lower than 5 m·s^{-1} (the corresponding superficial gas velocity was lower than 0.0064 m·s^{-1}), mixing of the gas and liquid phases in both the ingesting and expulsion parts caused the gas phase to break into a wide range of bubbles. Meanwhile, external sinusoidal pulsations resulted in water suck-back into the injector at a high gas velocity, causing the gas slugs to fragment intensely into tiny bubbles. With bubble breakup and the formation of smaller bubbles, the gas holdup and gas–liquid specific interfacial surface area increased,

Table 2
Summary of investigations on a bubble column with vibrating excitement.

Refs.	System	Dimension of column	Vibration type	Operating conditions	Gas sparger type	Investigated parameters	Key findings
Ellenberger et al. [64–67,72]	Air–water; air–water–silica	D = 100 mm, H = 4 m	Membrane-piston-exciter	f = 0–400 Hz, λ = 0–2.0 mm	Single capillary, 12 capillaries	Bubble diameter, gas holdup, mass transfer	40%–50% reduction of bubble diameter at 40–120 Hz; exist inflection point: f = 100 Hz, λ = 0.083 mm, gas holdup enhancement increased with amplitude monotonously and with frequency periodically, decreased with liquid height periodically; delay the transition to the churn-turbulent flow regime; enhancement factor independent of the slurry
Knopf et al. [68,69]	Air–water	D = 89 mm, H = 820 mm	Rubber-elastic/solid piston-eccentric cam	f = 0–30 Hz, λ = 0–2.54 mm	Single injector	Bubble breakup, gas holdup, mass transfer	Parabolic amplitude with frequency for elastic piston; monotonic amplitude for solid piston; power input and hydrodynamic instability induced bubble breakup
Waghmare et al. [70]	Air–CMC	D = 89 mm, H = 1060 mm	Rubber-solid piston-eccentric cam	f = 0–25 Hz, λ = 0–2.54 mm, ν = 1–62 cP	Single injector	Mass transfer, bubble force balance	Mass transfer coefficient decreased with the viscosity; $\frac{<k_La>\nu^{1/3}g^{1/3}}{U_g}=4.58\frac{\sqrt{D_0\nu_0}P_m^{4/5}}{(\sigma/\rho_l)^{6/5}}G(Bj)$; $G(Bj)=\frac{3}{2}\left[1-\frac{(1-Bj)^{2/3}}{Bj}\right]$
Budzyński et al. [71,73]	Air–water	D = 140 mm, H = 2250 mm	Membrane-piston-exciter	f = 0–100 Hz, λ = 0.25–2 mm, u_g = 1.6–13.9 m·s^{-1}	Single injector	Bubble diameter, gas holdup	$d_b=39.904\left(\frac{n_1Q}{\rho_l g}\right)^{3/4}\left(\frac{gU_g}{gU_g+4\pi^3X_p f_i^{*3}A_p/A_D}\right)$

All the symbols in this table are defined in the Nomenclatures list at the end of this paper.

and the mass-transfer process between phases was subsequently enhanced.

Several researchers [74,75] have focused on seeking a general theory to explain the experimental observations and provide guidance for the design, optimization, and scale-up of the pulsing bubble column. Waghmare et al. [70] developed a one-dimensional theory of the mass-transfer coefficient by taking the superficial gas velocity, liquid viscosity, and vibration frequency and amplitude as independent variables. The balance of the buoyancy and drag force exerted on gas bubbles in liquid pulsations could be achieved by considering three additional effects. The first effect is the Bjerknes force [70], which is caused by interactions between the forcing liquid and the pulsing bubbles. This is known as a kinetic buoyancy force acting in the opposite direction to the upward movements of the bubbles, resulting in a decrease of bubble rise velocity. The second effect is bubble breakage enhanced by pulsation based on the Hinze theory [74], which considers both the gas injection and the oscillation power. The third effect is the decrease in mass diffusivity resulting from the increase in liquid viscosity, which can be obtained according to the Stokes–Einstein equation. When these three effects were considered, the final prediction model of the mass-transfer coefficient provided a fairly reasonable alignment with the experimental data for the pulsation bubble column. Table 2 displays the correlation for predicting the volumetric mass-transfer coefficient. A defect of this model was its assumption that the amplitude of the liquid oscillation was equal to that of the exciter vibrations. In fact, it has been shown that the liquid oscillation amplitude is related to the types of vibration exciter [69]. With a correction based on the ratio of the gas injector power to the total power (including the injector and pulsation power), a prediction model of bubble size was deduced based on Davidson and Schuler's relation [71]. This correlation was successfully validated by experimental data with a deviation of 10%, as shown in Table 2.

According to the analysis mentioned above, the intensification of mass transfer between phases has two reasons. First, the presence of oscillations provides the bubbles with an additional downward Bjerknes force, leading to a decrease in bubble-rise velocity and an increase in gas–liquid contact time [70,71]. Second, vibrations introduced to the continuous phase enhance the breakage rates of bubbles in the bubble column. This promotes the formation of many smaller bubbles and magnifies the specific interfacial area for gas–liquid interactions. Finally, the mass transfer can be significantly improved by pulsations. This enhancement of mass transfer is related to the superficial gas velocity and the amplitude and frequency of the pulsations. There are usually optimum operating conditions under which great enhancement of the gas holdup and mass transfer can be achieved while requiring a low additional pulsation power. It should be noted that the type of pulsing piston can influence the amplitude of the liquid oscillation, and subsequently influence the bubble breakage dynamics.

2.1.3. Combinational process intensification

2.1.3.1. Multiple types of internals. A combination of perforated plates and straight tubes can reduce the overall back-mixing in a bubble column and provide relatively isothermal conditions, which is suitable for strongly exothermic reactions such as Fischer–Tropsch synthesis and methanol synthesis [76]. Maretto and Krishna [77] simulated the syngas conversion and productivity of the Fischer–Tropsch synthesis process in a multistage bubble column with a diameter of 7 m and a height of 30 m, and heat-exchange tubes. Fig. 6 [77] shows the schematic diagram. The flow regime of the gas phase was assumed as the plug flow in each stage, with the dense phase (i.e., slurry phase) remaining completely mixed under the isothermal condition. The modeling results demonstrated that the selectivity and productivity of the Fischer–Tropsch reaction notably increased with an increase in the number of perforated plates from 1 to 4, and the flow regime changed to plug flow when the number of sieves was greater than 4. Moreover, additional heat-exchange tubes needed to be installed to ensure the desired isothermal conditions in each compartment of the column.

2.1.3.2. Combination of different intensification methods. Installing orifice baffles and producing oscillations at a constant frequency are conventional methods for intensifying the mixing in bubble columns, as stated in Sections 2.1.1.2 and 2.1.2. A combination of these two methods has also been widely applied to intensify the hydrodynamics and mass transfer in column reactors. Table 3 [78–85] summarizes the research in this area.

Lucas et al. [78] applied an oscillatory baffled column reactor to the ozonation of wastewater containing *p*-hydroxybenzoic acid (*p*-HBA). In comparison with the results from a traditional bubble column, a 20% increase in the *p*-HBA degradation rate and a 4.5- to 5.0-fold increase in the *p*-HBA mineralization rate per mole of

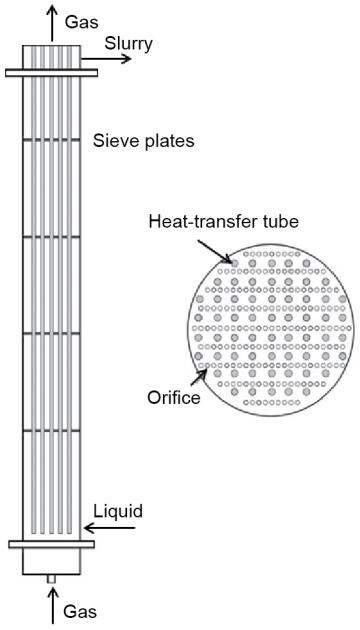

Fig. 6. Schematic diagram of a bubble column equipped with vertical tubes and sieve plates. Reproduced from Ref. [77] with permission of Elsevier Science B.V., ©2001.

ozone were obtained. The intensification of the ozonation process was attributed to the enhanced gas holdup and mass transfer due to the presence of orifice baffles and pulsations. Dissolution of carbon dioxide in the water was also enhanced by the use of a multi-orifice oscillatory baffled column [79]. It was shown that the baffle design parameters—including the orifice diameter, orifice number, and open area—had a significant effect on the bubble-size distribution and mass-transfer rate. Table 3 [78–85] illustrates the relevant investigations and the main conclusions or relationships that were obtained.

Five different types of oscillatory bubble columns, including a helical baffle reactor, smooth periodic constriction reactor, single-orifice baffled reactor, multi-orifice baffled reactor, and oscillatory bubble column reactor without baffles, were designed and investigated by Ahmed et al. [80]. The k_La in each oscillatory column reactor was diligently measured and compared for different oscillatory conditions and superficial gas velocities. It was demonstrated that a significant enhancement of the mass-transfer rate was obtained with the addition of orifice baffles and periodic constriction. Among these distinctive designs, the highest k_La was achieved in the oscillatory multi-orifice baffled reactor and was up to seven times higher than that in a reactor without baffles and oscillation under the same operating conditions.

Ni and Gao [81] first investigated the scale-up parameters in two different oscillatory baffled columns and obtained a correlation of k_La that adopted the power density as an independent variable, as shown in Table 3. It was found that there was an optimal baffle space where the vortices could be delivered without dispersion and suppression between the baffles. Their research indicated that the best baffle space was 1.8 times the tube diameter. Similarly, the optimal gas rate was obtained when the interfacial area reached a maximum without the occurrence of gas channeling. With an oscillatory frequency ranging from 2 to 6 Hz and an amplitude varying from 4 to 12 mm, the k_La monotonously increased with the pulsing frequency and amplitude. Oliveira et al. [82–84] investigated a pulsed baffle column with single-orifice baffles using a high-speed camera and inferred empirical relations between the gas holdup and bubble size, with power density as a

Table 3
Summary of investigations on oscillatory baffled bubble columns.

Ref.	System	Dimension of column	Sieve plates type	Oscillation	Operating conditions	Investigated parameters	Key findings
Lucas et al. [78]	Ozone–*p*-HBA	D = 150 mm, H = 540 mm	N_p = 31; N_o = 31; d_o = 10.5 mm; S = 40 mm	f = 2 Hz, λ = 10 mm	U_g = 1.98–4.43 mm·s^{-1}	Degradation rate	The degradation and mineralization rate of *p*-HBA increased
Pereira et al. [79]	CO_2–water	D = 150 mm, H = 540 mm	d_o = 6.4–30 mm; α = 15%–42%; S = 40–50 mm	f = 0–10 Hz, λ = 0–10 mm	U_g = 0.12–0.81 mm·s^{-1}	BSD, k_La	The modified oscillatory Reynolds number and Strouhal number were proposed for the design and scale-up
Ahmed et al. [80]	Air–water	D = 10 mm, H = 450 mm	Helical baffles; periodic construction; single orifice or multi-orifice plate	f = 0–10 Hz, λ = 0, 2, 4, 6, 8 mm	U_g = 0–21 mm·s^{-1}; Re = 0–8000	k_La	k_La: OMBR > OSBR > OIBR > OHBR > OR
Ni and Gao [81]	Air–water	D = 50 mm, H = 375 mm; D = 100 mm, H = 875 mm	N_p = 6; N_o = 23, d_o = 1 mm; N_o = 45, d_o = 1 mm	f = 3–8 Hz, λ = 4–12 mm	U_g = 2.12–8.49 mm·s^{-1}; U_g = 4.24–16.98 mm·s^{-1}	k_La	S/D = 1.8, $k_La = 0.0186(P/V)^{0.4}U_g^{0.32}$ (D = 50 mm); $k_La = 0.0256(P/V)^{0.425}U_g^{0.37}$ (D = 100 mm)
Oliveira et al. [82–84]	Air–water	D = 50 mm, H = 1.5 m	N_p = 14; single d_o = 24 mm; S = 75 mm	f = 1–5 Hz, λ = 2–8 mm	U_g = 1.06–6.37 mm·s^{-1}	BSD, ε_g, k_La, residence time	$d_{32} = 0.175U_g^{0.4}(P/V)^{-0.2}$; $\varepsilon_g = 0.1U_g^{0.4}(P/V)^{0.2}$; $k_La = 0.284\left(\varepsilon_g^{1.5}/d_{32}^{0.6}\right)$
Smith and Mackley [85]	Air–water	D = 24 mm, H = 1 m; D = 54 mm, H = 2 m; D = 150 mm, H = 4.5 m	S/D = 1.5	f = 1 Hz, λ = 1 mm, Q = 120 mL·min^{-1}; f = 0.0278 Hz, λ = 6 mm, Q = 720 mL·min^{-1}	Re_o = 10–3800	Axial dispersion	$E = 7\times10^{-7}Re^{0.8} + 7.5\times10^{-7}Re_o e^{-0.45Str} + \left(3\times10^{-12}Re^{1.6}\right)\Big/\left(7\times10^{-7}Re^{0.8} + 7.5\times10^{-7}Re_o e^{-0.45Str}\right)$

All the symbols in this table are defined in the Nomenclatures list at the end of this paper.
BSD: bubble size distribution; OMBR: oscillatory multi-orifice baffled reactor; OSBR: oscillatory single-orifice baffled reactor; OIBR: oscillatory integral baffled reactor; OHBR: oscillatory helical baffled reactor; OR: oscillatory reactor.

variable. Furthermore, the correlation of k_La was substantially improved, as shown in Table 3. Smith and Mackley [85] investigated the axial dispersion and liquid back-mixing in three oscillatory column reactors with different scales (i.e., 24, 54, and 150 mm) and deduced a correlation in which the axial dispersion was independent of the tube diameter under the conditions of a constant net flow Reynolds number (*Re*), oscillatory Reynolds number (Re_o), and Strouhal number (*Str*). The minimum axial dispersion occurred in the column when the value of $Re_o e^{-0.4Str}$ was equal to 1.37-fold $Re^{0.8}$.

2.1.4. General remarks

Numerous methods have been elaborated thus far, including equipping different internals, vibrating excitement, and combinational techniques to intensify bubble column performance. All of these intensification methods can be applied to promote gas holdup and mixing properties. Mass-transfer processes are intensified by these methods due to the generation of small bubbles, increase of the interfacial area, and generation of vortices.

For internal tubes, the enhancement of gas holdup increases with an increase in the occupation of the cross-sectional area. However, in regard to the influence of tube size on hydrodynamics, controversy still exists for different flow regimes. In a highly exothermic industrial process, internal tubes with 22%–25% occupation of the cross-sectional area are essential for heat exchange [35]. With the application of perforated plates, liquid back-mixing can be significantly reduced, and the liquid superficial velocity decreases with the decrease in open area. Static mixers installed in the reactor are applied to disperse large bubbles, resulting in an increase in the gas holdup and volumetric mass-transfer rate. Structured packing with a specialized design can also be used as static mixers and can simultaneously reduce undesirable back-mixing. Moreover, catalytic particles can be bound or loaded on the packing, and then equipped as a monolith in the reactor, eliminating the problems of liquid–solid separation. It has been estimated that structured packing could be applied in 25% of catalytic processes worldwide [86]. With the presence of oscillations at a constant frequency, the gas–liquid mass transfer is enhanced by the increase of the gas–liquid interfacial area resulting from the pulsation, and the contact time between gas and liquid can be extended due to the additional downward Bjerknes force. With the use of this vibrating excitement method, no additional intense liquid back-mixing or high shear—which should be avoided in some biotechnological processes—is induced in the reactor.

In comparison with a single intensification technique, a combination of different methods holds more potential for efficient process intensification from multiple aspects. It should be noted that no matter which method is adopted, the optimal process intensification can only be achieved using a suitable design and appropriate matching with the operating conditions in the bubble column.

2.2. Airlift loop reactor

Based on bubble column technology, the ALR was developed by installing concentric tubes, splitting a vessel into two vertical halves, or connecting two separated columns at the top and bottom. Compared with a bubble column, an ALR possesses better mixing ability, better energy-saving, and lower shear stress [87]. Thanks to these dominant advantages, the ALR has been widely employed in wastewater treatment, microbial fermentation, and Fischer–Tropsch synthesis [88]. To further improve ALR performance, numerous methods and techniques for process intensification have been continuously developed. The gas holdup, bubble-size distribution, mass transfer, mixing time, and extent of back-mixing are the principal parameters that determine the hydrodynamics, mass/heat transfer, and finally reactant conversion and selectivity in the reactor. Thus, the process intensification method focuses on these main parameters. Similar to the bubble column, internals insertion is one of the most common methods for process intensification in an ALR. The following sections concisely elaborate on the methods used for process intensification in the ALR.

2.2.1. Baffles

Baffles can be applied in ALRs to improve the mixing properties, enhance the mass-transfer rate, and transform the flow direction. In order to enhance the solids mixing, especially at the bottom of the column, and improve the heat exchange at the external wall in a photosynthetic process, helical flow promoters with an angle of 35° with respect to the column axis were installed in the downcomer of an ALR [89,90]. With these inserted helical baffles, radial mixing was enhanced by the helical movement of the gas–liquid–solid slurry, resulting in a more homogenous distribution of energy and suspended solid particles. Due to the resistance effects of the baffles, the liquid circulation time increased by less than 15% for both the water and dilute carboxy-methyl cellulose (CMC) solutions. Compared with a bubble column without internals, half of the gas flow rate was sufficient to arrive at a complete fluidization state with a helical flow promoter. The effects of solid concentration on the gas holdup, liquid velocity, and mass-transfer rate were thoroughly investigated. It was observed that the gas holdup and liquid velocity decreased slightly with an increase in the solid concentration. However, the gas–liquid volumetric mass-transfer rate decreased significantly. Quantitatively, with the addition of 206.5 $g \cdot L^{-1}$ of solid particles, the volumetric mass-transfer rates in water and in 0.2 wt% CMC solutions decreased by 37% and 47%, respectively. Based on substantial experimental data under different operating conditions, the empirical relations of the gas holdup, liquid velocity, and k_La with various influencing factors were summarized, as shown in Table 4 [17,90–97].

To observe the detailed flow structure and identify the flow trajectories in an IALR, Wu and Merchuk [98] applied an optical trajectory tracking system. Fluorescent particles were employed as tracers, and successive pictures were taken by two cameras connected to computers. This allowed the three-dimensional coordinates, velocity vector, and local shear strain rates of the tracer particles to be recorded and analyzed by digital image analysis; the flow paths were then drawn. Through this optical working system, the existence of secondary flow in an IALR with a helical promoter was first verified, and the mechanism of helix baffles improving radial mixing and heat exchange with the external walls was identified. Räsänen et al. [91] combined a helical flow promoter with a gas sparger to intensify the mixing and mass-transfer properties. They attached helical tubes with 0.6 mm needle to rotate on the outer side of the downcomer and/or on the inside of the riser column of the IALR. Different helical flow-promoter/gas sparger combinations were designed to investigate their influence on the hydrodynamics and mass-transfer rate. It was found that the gas holdup and k_La could be significantly promoted without additional energy input. The value of k_La for oxygen could be increased threefold by the use of both a helical flow-promoter and gas sparger, compared with that in an IALR without internals.

In addition to enhancing the hydrodynamics using helical internals, baffles of different configurations can be applied to guide the flow in the column. Pi et al. [99] equipped a trumpet-shaped hood above the internal tube in an ALR. They found that the liquid circulated in two-layer cyclic routes both below and above the hood, and that an extra circulating route was formed in a suitable installation position. With the trumpet-shaped riser and an imaged riser, the flow structure tended to be more uniform and the dead space in the reactor decreased. With the installation of this novel riser,

Table 4
Summary of theoretical and empirical correlations in intensified ALRs.

Ref.	Reactor type	Empirical relations	Operating conditions
Schlötelburg et al. [90]	Helical flow promoters–IALR	$U_l = 0.25U_g^{0.33}(A_d/A_r)^{0.78}\mu_{slurry}^{-0.29}(1-\varepsilon_s)^{0.74}$, $k_La = 0.00422U_g^{0.876}(1-\phi_s)^{2.44}\mu_{slurry}^{-0.286}$	$0 \le \varepsilon_s \le 0.1881$
Räsänen et al. [91]	Helical flow promoters–gas sparger IALR	$k_La = c_1(U_{gsr}/U_{gsr,avg})^{c_2}(1+U_{gsd}/U_{gsd,avg})^{c_3}$, $Sh = 29.1187 \pm 17.8016(Fr_r/Fr_{ravg})^{0.9076\pm0.1667}\cdot\left[1+(Fr_d/Fr_{davg})^{0.4495\pm0.0527}\cdot\varepsilon_g^{1.1184\pm0.2346}\right]$	$0.013\ m\cdot s^{-1} \le U_g \le 0.035\ m\cdot s^{-1}$
Luo et al. [92]	Sieve plates–IALR	$\varepsilon_g = 107.72d_0^{-0.21}\alpha^{-0.16}n^{0.21}U_g^{0.75}$, $k_La = 0.35d^{0.19}\alpha^{0.13}n^{0.48}U_g^{0.86}$	$0.000877\ m\cdot s^{-1} \le U_g \le 0.00281\ m\cdot s^{-1}$, $2.5\ mm \le d \le 3.5\ mm$, $0.37 \le \alpha \le 0.73$, $1 \le n \le 2$
Zheng et al. [93]	Helical sieve plates–IALR	$\varepsilon_g = 1.766U_g^{1.009}\theta^{0.008}\left[0.85-(0.798-\alpha)^2\right]^{0.199}$, $k_La = 1.989U_g^{0.958}\theta^{0.018}\left[0.798-(0.778-\alpha)^2\right]^{1.42}$ (riser), $k_La = 1.722U_g^{1.098}\theta^{0.078}\left[0.798-(0.778-\alpha)^2\right]^{1.037}$ (downcomer), $k_La = 1.869U_g^{1.005}\theta^{0.039}\left[0.798-(0.778-\alpha)^2\right]^{1.285}$ (overall)	$0.009\ m\cdot s^{-1} \le U_g \le 0.09\ m\cdot s^{-1}$, $10° \le \theta \le 31°$, $35\% \le \omega \le 63\%$
Chisti et al. [94]	Static mixers–EALR	$\varepsilon_g = U_g/[A+B(U_g+U_l)]$	–
Goto and Gaspillo [95]	Static mixers–EALR	$Sh = 2 + b_1\left(U_g g d_s^4/\mu^3\right)^{b_2}Sc^{1/3}$	–
Lu et al. [96]	Static mixers–EALR	$k_La = 0.0003\mu_{slurry}^{-0.348}\left(P_A^{0.388}+P_P^{0.293}\right)$ (without static mixers), $k_La = 0.0003\mu_{slurry}^{-0.316}\left(P_A^{0.413}+P_P^{0.308}\right)$ (with static mixers)	–
Meng et al. [97]	Packed bed–EALR	$\varepsilon_g = (-2.75+0.272h_p+4.03\phi)U_g^{0.701}(1+U_0)^{0.379}$, $U_{LR} = (-54.3-7.53h_p+71.4\phi)\left[\frac{\varepsilon_g}{(1-\varepsilon_g)^{-2}+(A_r/A_d)^2}\right]^{0.92}$, $k_La = 0.531U_g^{0.761}$	$0.0031\ m\cdot s^{-1} \le U_g \le 0.016\ m\cdot s^{-1}$, $0.9 \le \phi \le 1$, $0 \le h_p \le 1.2\ m$
Lukić et al. [17]	Impeller–EALR	$k_La = p_1U_g^{p_2}d_0^{p_3/U_g}[1+(-d\sigma/dC)]^{p_4}$ (nonviscous), $k_La = p_1U_g^{p_2}d_0^{p_3/U_g}\mu_{eff}^{p_5}$ (viscous)	Nonviscous: $p_1 = 0.152$, $p_2 = 0.74$, $p_3 = -0.00263$, $p_4 = -0.67$ (no impeller); $p_1 = 0.169$, $p_2 = 0.71$, $p_3 = -0.0023$, $p_4 = -0.66$ (impeller); viscous: $p_1 = 0.00944$, $p_2 = 0.64$, $p_3 = -0.00394$, $p_4 = 14.4$, $p_5 = -0.3$ (no impeller); $p_1 = 0.00797$, $p_2 = 0.62$, $p_3 = -4.58$, $p_4 = 14.1$, $p_5 = -0.36$ (impeller)

All the symbols in this table are defined in the Nomenclatures list at the end of this paper.

the overall gas holdup and k_La were enhanced by 16.2% and 10.2%, respectively. Li et al. [18] set an inverted bell-shaped internal between two stages in a two-stage IALR. The slurry from the riser of the bottom stage was compressed into the second stage with the constriction of the internals, resulting in greater gas holdup in the upper stage. Different bubble circulation regimes existed in the two stages of the reactor under the low superficial gas velocity; that is, a complete bubble circulation regime occurred in the first stage while a transition regime occurred in the second stage. With an increase in the superficial gas velocity and solid concentration, the bubble circulation gradually transformed into a complete circulation regime. It was reported that the axial distribution of the solid concentration tended to be homogeneous when the superficial gas velocity and solid loading were increased in the whole reactor.

2.2.2. Perforated plates

Horizontal perforated plates with multiple orifices have been demonstrated to be an efficient method to induce bubble breakup and enhance the mixing extent in aerated reactors. Krichnavaruk and Pavasant [100] investigated the influence of sieve plates with different pore diameters and pore numbers on the k_La, gas holdup, and riser liquid velocity. It was found that the value of the k_La increased to as much as double, compared with the value without perforated plates. This substantial improvement in the k_La was attributed to the increase of the gas–liquid interfacial area with frequent bubble breakup by the sieve plates. Nevertheless, the gas–liquid mass-transfer coefficient (k_L) decreased when perforated plates were installed because of the decreased liquid-circulation velocity resulted from the hindrance caused by the sieve plates in the flow pathway. These two contrary effects made it difficult to create an optimal design of the sieve plates in order to achieve the highest improvement of k_La. In that study, it was observed that three perforated plates with 21 holes that were 4 mm in diameter were the best choice to increase the k_La at a superficial gas velocity ranging from 1.889 to 7.515 $cm\cdot s^{-1}$.

Luo et al. [92] reported that a larger orifice diameter on the sieve plates, varying from 2.5 to 4.5 mm, provided greater enhancement of the k_La for the same free area ratio. This phenomenon was attributed to two aspects. First, with a smaller pore diameter, large bubbles tended to congregate to form a bubble layer below the sieve plates, which led to a decrease of the gas–liquid interfacial area. Second, the flow resistance was strengthened with the decrease in sieve diameter, resulting in a greater decrease in liquid velocity. Furthermore, correlations of the overall gas holdup and k_La related to the sieve plate structural parameters and operating conditions were derived based on the experimental data, as shown in Table 4.

Aside from the significant intensification techniques discussed above, Vorapongsathorn et al. [101] reported that perforated plates (smaller than the riser cross-section) with eight 3 mm holes placed along the riser of the IALR slightly improved the gas holdup and k_La. This was ascribed to the fact that the orifice plate occupied only half of the riser sectional area, with a fairly small open area. When these perforated plates were equipped, the fluids flowed around the sieve plates following a path of lower resistance. Under

these circumstances, the internals had a limited positive influence on the hydrodynamics, except for acting as a hindrance to the fluid. Thus, these findings indicated that a suitable perforated plate design was crucial to positively enhance the hydrodynamics in a pneumatically agitated reactor.

Zhang et al. [102] set up a novel perforated internal structure containing baffles maintained at 45° with the vertical axis in the riser tube of an EALR. The influence of these internals on the bubble Sauter diameter and rise velocity, as well as on the local gas holdup and its radial distribution, was investigated by comparing the hydrodynamics before and after the installation of sieve plates. It was verified that the perforated plates enhanced the gas holdup, narrowed the bubble-size distribution, and reduced the radial maldistribution. Nevertheless, the influence of the internals on the hydrodynamics in that study was effective only for a limited distance of about 1.1 m above the sieve plate.

Zheng et al. [93] assembled helical sieve plates in the riser of an IALR. With the helical plates, the gas holdup was enhanced by 38%–63% in comparison with that of a setup without plates. The researchers proposed that the enhancement was independent of the free area ratio, which ranged from 35% to 63%, and the helix angle, which ranged from 10° to 31°. Similar to the effect of planar sieve plates, the bubble diameter was decreased, and there was a more uniform size distribution due to frequent bubble breakup through the plates, which occurred every time. As a result, the gas–liquid interfacial area increased, and the volumetric mass transfer was improved. Quantitatively, the k_La increased by about 20% with the use of helical sieve plates in the IALR, in comparison with an empty IALR. Empirical correlations of the gas holdup and k_La, with the influences of the superficial gas velocity, free area ratio, and helical angle, were deduced by fitting the experimental data by the least square method. Table 4 summarizes these empirical equations and valid ranges. It was shown that the homogenous flow regime of the IALR was broadened with the use of helix sieve plates. The mixing time was extended due to the space partition and resistance to the gas–liquid flow provided by the helical plates, while the tangential mixing performance was improved. This phenomenon was also observed in the ALR assembly with a helical promoter in the downcomer [89,90].

Perforated plates can also be applied between stages in multistage ALRs. Yu et al. [103,104] designed a perforated plate equipped not only with multiple orifices but also with three long tubes to improve the distribution of solid particles and to avoid liquid flooding in the column. It was found that the novel inter-stage internals separated the gas–liquid–solid slurry flow into two parts: The gas flowed upward through the orifices, as in an ALR with traditional sieve plates, while the liquid and solids flowed upward through the tubes. The flow regime and gas layer height below the sieve plates were significantly influenced by the superficial gas velocity and the opening area of the gas orifice for both the co-current and countercurrent flow. The gas layer height should be strictly controlled within an appropriate range when the slurry flow circulates normally within each stage.

The effects of various configurations of perforated plates (i.e., planar or helical) with different open areas and orifice diameters on the hydrodynamics and mass-transfer properties in ALRs have been investigated under a wide range of operational conditions. Due to contrary influences such as bubble breakup and flow resistance, a suitable design of the equipped sieve plates is a key parameter for positive process intensification. Thus, a suitable design and mounting position should be carefully considered in order to achieve the desired purpose.

2.2.3. Static mixers or packed beds

As discussed in Section 2.1.1.3, static mixers have been widely employed to intensify the hydrodynamics and interphase mass transfer, due to their enhancement of the bubble breakup and flow disturbance. Likewise, static mixers can be applied in ALRs to achieve similar effects [96]. Chisti et al. [94] conducted experiments in an EALR equipped with static mixers in the riser and demonstrated that the k_La could be significantly enhanced by static mixers. Furthermore, the k_La enhancement increased with an increase in fluid viscosity because larger gas bubbles coalesced more easily in viscous liquid without motionless internals. Quantitatively, the k_La was enhanced up to sixfold compared with that in the same setup without static mixers in a NaCl solution with 0.6% w/v (gram per 100 mL) CMC. Prominent enhancement of the k_La by static mixers in the riser was also observed by Goto and Gaspillo [95] in a gas–liquid–solid system. Their results showed that the minimum gas velocity required to completely suspend the solid was decreased by about 30% when static mixers were used, which is beneficial for extending the application range of an EALR. Table 4 shows the related empirical correlations based on the experimental data.

Packed beds have been widely applied as a support for catalysts or immobilized microorganisms and enzymes in multiphase chemical reactors [58]. Porous materials, such as fibrous cotton, glass, nylon, and polymer foam, have been identified as suitable for packing in aerated reactors, due to their high specific surface area, low mass-transfer resistance, and small pressure drops [105,106]. Meng et al. [97] and Nikakhtari and Hill [107] thoroughly investigated the hydrodynamics and mass-transfer properties in EALRs equipped with woven nylon packing. With the placement of mesh packing internals, the bubble Sauter diameter decreased significantly due to frequent bubble breakup. It should be noted that only an appropriate arrangement of the porosity and height of the packed bed resulted in a positive enhancement of the hydrodynamic properties. When the packing porosity was 0.9, the gas holdup in the column was decreased by installing the packing internals. In that study, the maximum gas holdup was obtained with a porosity of 0.99. When the packing porosity was increased, the gas holdup and liquid velocity in the riser increased monotonously. The liquid velocity in the riser decreased with increasing packing height, while the gas holdup was nearly invariant. With a packing porosity of 0.99 and a packing height of 1.2 m, the gas holdup and k_La between oxygen and water at a superficial gas velocity of 0.005 $m{\cdot}s^{-1}$ were improved by about 74% and 174%, respectively. For the volatile organic chemicals toluene and benzene, the overall k_La was enhanced on average by 65.1% and 33.4%, respectively [108]. This novel packed bed has also been reported to be efficient for the bioremediation of phenol-polluted air steam, with all the phenol being totally removed at one-third of the height of the bubble column [109].

Mixing properties versus superficial liquid velocity were explored using non-intrusive electrical resistance tomography in a circulated EALR with equipped two-stage packing internals and a gas redistributor [110]. It was reported that the liquid velocity decreased with the installation of packing and a gas redistributor, due to hindrance from the internals [111]. Correspondingly, the mixing time increased by up to 44% with one bed of packing and further increased by 270% with the combination of two beds of packing and a gas redistributor, because the resistance of the liquid flow was significantly increased. Moreover, the overall gas holdup increased by about 36% due to the bubble breakup and fluid resistance [112]. Ultimately, the k_La was clearly enhanced because of the improved gas dispersion.

2.2.4. Mechanical internals

Mechanical internals, such as blades or impellers, have been extensively applied in stirred tanks and bubble columns to intensify the mixing properties [113,114]. In addition, mechanical impellers can be applied in an IALR in combination with static

mixers [96]. The influences of agitation speed and static mixer length on the gas holdup, liquid velocity, and k_La were thoroughly investigated by Lu et al. [96]. It was found that the k_La enhancement derived from the mechanical impeller was greater than that derived from the static mixers in a highly viscous fluid system. It should be noted that most of the studied mechanical impellers were motor-driven, requiring significant additional energy input.

With an appropriate design of the shafts and impellers, a novel IALR inserted with constructed self-agitated impellers was established, and its hydrodynamics and mass transfer coefficient were explored [115]. Fig. 7 [115] provides a schematic diagram of the IALR. The number and arrangement of impellers were carefully chosen in order to have them be agitated only by the gas throughput and liquid circulation. It was observed that the impellers in the riser of the IALR began rotating under an extremely low gas superficial velocity of 0.00629 $m{\cdot}s^{-1}$. With an increase of the superficial gas velocity, the rotating speed first increased and then tended to remain at a relatively constant value when the superficial gas velocity was above 0.45 $m{\cdot}s^{-1}$. With the installation of impellers, the gas holdup in the riser increased by about 45%. The enhancement of the gas holdup in the riser was 25%–48% greater than that induced by certain other internals, such as baffles [101] and perforated plates [100]. In contrast, the enhancement of the overall gas holdup was insignificant, due to the offset effects in the downcomer. Based on this research, Lukić et al. [17,116] built a novel EALR with self-agitated impellers inserted in the riser. They observed that the k_La was enhanced by up to 82% under a low superficial gas velocity (about 0.01 $m{\cdot}s^{-1}$), while the value of the k_La increased by 20%–30% under higher aerated conditions. The reduced improvement in the k_La when the superficial gas velocity increased was attributed to a decrease in impeller efficiency.

2.2.5. General remarks

As in bubble columns, equipping various internals is the most common method to intensify the mixing and transfer performance in ALRs. Helical baffles are inserted to enhance the radial mixing, resulting in a more homogeneous distribution of suspended solid particles and energy (heat or light). Baffles with a special design (trumpet-shaped, bell-shaped, etc.) equipped at the top or between stages in an ALR also help to guide the flow pattern. When perforated plates are installed, the volumetric mass-transfer rate is promoted due to the formation of small bubbles, while flow resistance exists due to the hindrance presented by the sieve plates. Static mixers also enhance the mass transfer due to bubble breakup, while the problem of flow hindrance cannot be ignored. A packed bed can be applied as a catalyst support, and the liquid–solid separation unit in the gas–liquid–solid system can then be removed. In mechanical internals with an appropriate design, enhancement of the gas holdup is generally greater than those in other internals, especially in a highly viscous system. Nevertheless, it should be noted that high shear is induced by impellers. Similar to intensification methods in bubble columns, only an appropriate design of the internals, shape, angle, position, and so forth can result in optimal improvement in an ALR.

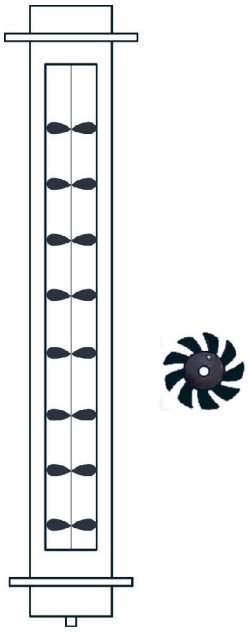

Fig. 7. Schematic diagram of an IALR equipped with self-agitated impellers [115].

3. Process intensification of mixing and separation

One of the major challenges in improving ALR performance is the efficient separation of solids from liquids in three-phase working systems. A considerable number of investigations have been conducted on separating solid catalyst particles from the liquid product to achieve high efficiency and low energy consumption.

3.1. Settling

Compared with the solid catalysts in fixed beds, which usually have a particle diameter greater than 1 mm, the solid particles in slurry reactors typically range from 10 to 200 μm in diameter [25,26]. The particles in the slurry can be easily separated by settling. Benham et al. [117] reported that a passive dynamic settler could be applied to divide the catalysts from a wax product in the downcomer of an EALR without a pump. The catalysts were delivered back to the column below the settler, with the light wax products being collected at the overflow. Unfortunately, the separation mechanism of the dynamic settler was not clearly presented.

The solid particles in most slurry reactors have diameters ranging from 20 to 200 μm [118,119] and can be cheaply separated using a hydrocyclone [120]. Based on this fact, Yang et al. [25] proposed a continuous separation technique in an IALR, in which a compact, efficient, and energy-efficient hydrocyclone [121] was equipped in the bottom of the downcomer. Through this built-in separating device, clear liquid products were collected from the overflow of the hydrocyclone, with dense slurry catalysts concentrated at the underflow and continually circulated in the reactor. The division of clear liquid from the concentrated slurry in the hydrocyclone was accomplished by two driving forces: first, the hydraulic potential energy derived from the altitude difference between the liquid level and the hydrocyclone inlet; second, the kinetic energy of the slurry at the hydrocyclone entrance. It was shown that the distribution of solid particles inside the reactor varied slightly for four hours of operation in this novel slurry reactor, indicating that quite clean liquid products were obtained at the overflow, with few solid catalysts entrained. During this process, clear products were obtained, and a continuous catalytic reaction was ensured with no extra energy consumption. Therefore, a considerable amount of capital costs (including an expensive slurry pump, solids feeder, and pipes) and operating costs (including electric charges for the liquid–solid separation and solids feeding, and maintenance costs of moving devices) can be saved. Moreover, catalyst attrition can be reduced due to suspension by the continuous liquid phase, and catalyst deactivation due to a broken catalyst can be effectively prevented. It has been demonstrated that this new slurry reactor with an elaborate design functions very well when employing solid particles with an appropriate particle-size

distribution and density. Process intensification of separation and mixing has also been applied in an EALR; Fig. 8 illustrates the schematic diagram of this reactor.

3.2. Filtration

Filtration is one of the simplest and most convenient methods for separating solids from liquid flow. Rytter et al. [122] reported on a bubble column with a filtration element installed, which was free of catalysts, for separating the liquid products from the slurry. A constant-level controller was placed inside the filter unit to maintain a constant filtrate level below the slurry. The stable pressure differential between the slurry and the filtration device drove the slurry into the element for separation. Jager et al. [123] also set filters inside a bubble column with a back-flushed device to prevent blocking of the filtration medium. Anderson [124] described a separation method for a liquid product and solid catalyst using a novel internal microfilter with three parts: a porous reactor-side metal-cylinder outer surface, a porous reactor-side metal-cylinder inner surface, and a filter medium. Moreover, the outer and inner surfaces had a greater porosity than the filter medium. With this filter, catalysts with diameters from 0.5 to 100 μm could be separated from wax products inside the slurry reactor.

3.3. Composite methods

In order to obtain a clear liquid product by separating solid particles from the slurry, Clerici and Belmonte [125] developed a hydrocyclone combined with single or multiple filtration units. After coarse separation by the hydrocyclone, the overflow containing fine particles was further separated by a micro/ultrafiltration element. The concentrated slurry from the underflow of the hydrocyclone and the filtration units flowed back to the reactor through the outboard pipeline. White et al. [126] described a method for separating a wax product from the catalysts by combining extraction with settling. The slurry was first delivered to a stationary mixer to extract the organic products and was then pumped to a centrifugal separator for further separation. An additional separator was highly desired for the substantial segregation of the catalyst particles. Hu et al. [127,128] combined settling and filtration for continuous solid–liquid separation in a bubble column and achieved high efficiency and long-term stable operation.

Fig. 8. Schematic diagram of an external loop slurry reactor integrating mixing and separation.

Settling, which is induced by gravity or by centrifugal force, is one of the most common primary liquid–solid separation methods. Although filtration can be used for relatively complete separation, it often requires considerable energy input and introduces the problem of blocking. For the complete separation of a wax product and solid catalysts, a combination of different separation schemes is usually essential. Moreover, the separation method should be selected appropriately based on the chemical and physical properties of the slurry.

4. Additional design considerations and challenges

4.1. Flow regime

Similar to a gas–liquid system, the hydrodynamics in industrial pneumatically agitated slurry reactors are characterized by three typical flow regimes: homogeneous (bubbly flow), transitional, and heterogeneous (churn-turbulent flow) regimes, mainly depending on the superficial gas velocity employed [8,26,87]. The flow regimes in the reactor feature different bubble-size distributions, from which the flow patterns can be discriminated. In a homogeneous regime, the superficial gas velocity is relatively low and the bubble size is small (1–7 mm in diameter [76,129]); a narrow bubble-size distribution is manifested, and the coalescence and breakup phenomena are correspondingly negligible due to minor bubble–bubble interaction. At a higher gas velocity, some large bubbles (20–70 mm in diameter [76,129]) are present due to bubble coalescence, and then a heterogeneous regime is developed; a wide bubble-size distribution is demonstrated, and coalescence and breakup phenomena are notable. These two regimes are bordered by a transition regime.

It is vital to understand the hydrodynamic characteristics in slurry reactors under different flow regimes for the purposes of proper design, operation, control, and scale-up. In the last decades, many studies have been dedicated to the regime transition. Several methods for identifying the transition in the flow regime have been put forward, and details can be found in the related literature [8,26,87]. It is notable that although there are publications on the regime transition for the gas–liquid two-phase flow, charts of the flow regime for the gas–liquid–solid three-phase flow are very scarce, especially for high solid concentrations. In a homogeneous regime, the gas holdup in the reactor increases linearly with an increase of the superficial gas velocity, and the line of the gas holdup versus the superficial gas velocity passes through the origin with a slope greater than or close to 1 [8,130]. However, for a heterogeneous flow regime, the slope is markedly suppressed due to large-bubble formation. Both the experimental and numerical results indicate that large bubbles mainly ascend in the central region of the column with large rise velocities, while small bubbles were much more uniform in the whole cross-section [26]. Therefore, the radial profile of the gas holdup in the column is relatively uniform in a homogeneous regime, while it becomes parabolic in a heterogeneous regime.

Gas-agitated slurry reactors can be operated in both the homogeneous flow regime and heterogeneous flow regime [131]. In the heterogeneous regime, the small bubbles coalesce into large bubbles, which rise up at high velocities in a plug-flow manner. Under these circumstances, there is no axial mixing for the large bubbles, while the small bubbles have the same back-mixing characteristics as that in the slurry phase. Therefore, the heterogeneous flow regime has been thought to be the most optimal condition for the Fischer–Tropsch synthesis [132].

It should be pointed out that the flow regime depends not only on the reactor design parameters (i.e., distributor design and column diameter), but also on the operating parameters (i.e., superficial gas and liquid velocity, temperature, and pressure) and the physical properties of the working system (i.e., liquid viscosity, solid holdup, surface tension, density, and coalescing nature of the liquid phase) [133,134]. It is noteworthy that when a poor gas distributor was used, heterogeneous regimes prevailed at all the superficial gas velocities [8]. Van Baten and Krishna [135] found that when the solid particle concentrations exceeded 30 vol%, fast-rising large bubbles belonging to the spherical cap family occurred almost exclusively.

4.2. Gas sparger

The initial gas bubble size in a slurry reactor column is strongly affected by the gas sparger, which in turn influences the bubble-size distribution, gas holdup, and mass-transfer properties in the slurry reactor. Commonly applied types of gas sparger include single-orifice, sinter plate, perforated plate, porous plate, membrane, ring-type, and arm-type distributors. The spatial arrangement and orifice diameter of the gas sparger have been shown to influence the gas holdup in the reactor [136]. It has been indicated that higher orifice numbers with smaller orifice diameters show better performance in mass transfer [137]. It is noteworthy that bubble formation at multiple submerged orifices in a gas–liquid apparatus under industrial jetting conditions has been systematically investigated. A simple correlation of the influence of the orifice diameter, orifice superficial gas velocity, and liquid properties on the initial bubble diameter was proposed and was validated against extensive experimental data [138].

For the design of a gas sparger, Lin et al. [139] investigated the radial distribution of the gas holdup and bubble size in EALRs equipped with gas distributors of porous plates and perforated plates. It was shown that different radial profiles of the gas holdup were obtained—that is, a wall-peaking profile was obtained for a column with a porous sinter plate distributor, and a core-peaking profile was obtained for a perforated plate distributor. Wei et al. [140] stated that a novel membrane-tube sparger with a bunch of porous cylindrical tubes enhanced the overall gas holdup by as much as 48.8% under a superficial gas velocity ranging from 0.004 to 0.04 $m{\cdot}s^{-1}$ in an air–water system, with an improvement of the k_La of up to 84.4%.

Aside from hydrodynamics and mass transfer, the flow structure in the column can be affected by the gas sparger design. Hooshyar et al. [141,142] adopted a structured gas distributor with a uniform needle sparger in order to structure the flow pattern and reduce back-mixing in the slurry bubble column reactors. It was shown that when applying this sparger, vortical structures were significantly reduced and the homogeneous regime was broadened. Vial et al. [12,143] investigated the flow regime in EALRs equipped with single-orifice, multiple-orifice, and porous-plate gas spargers through pressure fluctuations analysis. It was shown that the column with a single orifice always operated in the heterogeneous regime with a superficial gas velocity (U_g) ranging from 0.01 to 0.24 $m{\cdot}s^{-1}$. For the multiple-orifice sparger, the heterogeneous regime was achieved at a U_g of about 0.11 $m{\cdot}s^{-1}$. Nevertheless, the transition velocity was dependent on the start-up method for the column. A heterogeneous flow pattern in a column using porous plate with a "dry" start-up was reached when the superficial gas velocity was about 0.11 $m{\cdot}s^{-1}$ (i.e., the same value by using a multiple-orifice distributor), whereas it was reached after about 0.07 $m{\cdot}s^{-1}$ with a "wet" start-up.

The extent of the influence of the gas sparger on the hydrodynamics and transfer properties is related to the structural and operational conditions. Cao et al. [144] argued that sparger design had a noticeable effect on the gas holdup and axial dispersion at a low superficial gas velocity (U_g < 0.025 $m{\cdot}s^{-1}$) with a low solid volume fraction (ϕ_s < 2%), while slight effects were found at a high superficial gas velocity and high solid loading. It is the consensus that sparger design remarkably affects the hydrodynamics in a bubbly flow regime but only affects the region around the distributor in a churn-turbulent flow regime [145]. Michele and Hempel [146] indicated that the sparger influence was more pronounced at low superficial gas velocities than at higher ones because large bubbles commonly formed at high superficial gas velocities regardless of the sparger type.

Generally speaking, for porous-type gas distributors, the pores in the plate or tubes are usually designed to be large enough for the passage of gas yet small enough to keep solid particles from leaking through the pores. However, severe pore clogging may occur due to solid particle attrition or failure of the gas supply [26]. For an industrial slurry reactor operating in the heterogeneous regime with a high superficial gas velocity and a high solid concentration, the ring-type distributor and arm-type distributor have been recommended, and some holes facing downward are highly desired to ensure a full solid suspension and clean discharge [147,148]. When operating at a low superficial gas velocity, a gas sparger with small orifices, such as a porous-plate, perforated-plate, or membrane sparger, is preferred for high efficiency. It should be noted that the initial bubble size increases with an increase in solid volume fraction [149], and severe problems of mixing and mass/heat transfer may arise at high solid volume fractions [147].

4.3. Influence of solid particles

For industrial pneumatically agitated slurry reactors, the solid volume fraction in the column usually ranges from 15% to 30%, and can even go up to 50% [150]. The presence of solid particles has a significant influence on the bubble size and distribution, bubble-rising velocity, gas holdup, and flow regime transition, which are pivotal parameters for mass- and heat-transfer properties [151–153]. Although extensive studies have been conducted to investigate the effects of solid particles on the hydrodynamics and transfer efficiency in slurry reactors, the underlying mechanisms are still not clarified due to their complexity.

For particles in the slurry that have a diameter smaller than 100 μm, the solids can be easily suspended in the liquid phase without the problem of particle settling [26]. Therefore, the slurry phase in the reactor can be simplified by assuming the liquids and solids to be in a pseudo-slurry phase, and the main influence of the solid concentration can be taken as an increase in the apparent viscosity of the liquid phase. In order to predict the hydrodynamics in slurry reactors using the apparent physical properties, numerous empirical and theoretical correlations of the effective viscosity have been proposed, as shown in Table 5 [154–169]. For a dilute suspension of solids, Einstein first proposed a correlation of the effective slurry viscosity based on the liquid viscosity and solid concentration; that is, $\mu_{slurry} = \mu_l(1 + 2.5\phi_s)$. However, this is only suitable for extremely low loading of solid particles (i.e., ϕ_s is up to 0.01) because it neglects the hydrodynamic interactions. For a concentrated solids suspension in a slurry reactor, the relative viscosity (μ_{slurry}/μ_l) is commonly expressed as a polynomial function with solid concentration as an independent variable in order to extend the application range. The value of each coefficient, which reflects the rotation, collisions, and hydrodynamic interactions of the solids, is fitted using experimental data. Thus, different empirical correlations are achieved due to various operating conditions and physical properties [154]. Furthermore, several phenomenal and theoretical relations have been proposed, with validation against experimental results [155,156]. However, as pointed out by

Table 5
Theoretical and empirical correlations of the slurry's apparent viscosity.

Refs.	Correlation	Remarks
Guth and Simha [154]	$\mu_{slurry} = \mu_l\left(1 + 2.5\phi_s + 14.1\phi_s^2\right)$	
Vand [155]	$\mu_{slurry} = \mu_l \Big/ \left(1 - 1.1\phi_s - 0.97\phi_s^2\right)^{2.5}$	$\phi_s \leq 0.5$, rigid sphere, without binary collision effects
Roscoe [156]; Brinkman [157]	$\mu_{slurry} = \mu_l(1 - 1.35\phi_s)^{-2.5}$	$\phi_s \leq 74$, rigid sphere
Bakopoulos [158]	$\mu_{slurry} = \mu_l[1 + (\rho_s + \rho_l)/\rho_l](1 - \phi_s)^{-2.59}$	$d_s < 10$ μm, non-settling slurry
Thomas [159]	$\mu_{slurry} = \mu_l\left(1 + 2.5\phi_s + 10.05\phi_s^2 + 0.0273e^{16.6\phi_s}\right)$	$0 \leq \phi_s \leq 0.6$
Ford [160]	$\mu_{slurry} = \mu_l\left(1 - 2.5\phi_s + 11.0\phi_s^2 - 11.5\phi_s^7\right)$	$0 \leq \phi_s \leq 0.52$
Eilers [161]	$\mu_{slurry} = \mu_l\left[1 + 1.25\phi_s/(1 - \phi_s/\phi_{s,max})\right]^2$	$\phi_{s,max} = 0.74$
Chong et al. [162]	$\mu_{slurry} = \mu_l\left(1 + 0.75\dfrac{\phi_s/\phi_{s,max}}{1 - \phi_s/\phi_{s,max}}\right)^2$	$\phi_{s,max}$ = 0.605–0.74
Fedors [163]	$\mu_{slurry} = \mu_l\left[1 + 1.25\phi_s/(\phi_{s,max} - \phi_s)\right]$	$\phi_{s,max}$ = 0.63–0.68
Frankel and Acrivos [164]	$\mu_{slurry} = \frac{9}{8}\mu_l\dfrac{(\phi_s/\phi_{s,max})^{1/3}}{1 - (\phi_s/\phi_{s,max})^{1/3}}$	$\phi_s \leq 0.8$
Quemada [165]	$\mu_{slurry} = \mu_l(1 - \phi_s/\phi_{s,max})^{-2}$	Fully dispersed
Mooney [166]	$\mu_{slurry} = \mu_l e^{\frac{2.5\phi_s}{1 - \lambda_1\phi_s}}$	Monodisperse system, Newtonian fluids
Kawase and Ulbrecht [167]	$\mu_{slurry} = \mu_l\dfrac{1 + 8.203\phi_s^5}{1 - 2.478\phi_s + 18.456\phi_s^5 - 20.326\phi_s^6}$	Non-Newtonian fluids
Krieger and Dougherty [168]	$\mu_{slurry} = \mu_l e^{\left(1 - \phi_s/\phi_{s,max}\right)^{-2.5\phi_{s,max}}}$	Rigid sphere, non-Newtonian fluids
Sengun and Probstein [169]	$\mu_{slurry} = \mu_l\left\{1 + C\frac{3\pi}{8}\frac{\beta}{1+\beta}\left[\frac{3+4.5\beta+\beta^2}{\beta+1} - 3\frac{\beta+1}{\beta}\ln(\beta+1)\right]\right\}$, $\beta = \dfrac{(\phi_s/\phi_{s,max})^{1/3}}{1 - (\phi_s/\phi_{s,max})^{1/3}}$	$\phi_s > 0.25$

All the symbols in this table are defined in the Nomenclatures list at the end of this paper.

Rabha et al. [170], the assumption of a pseudo-homogeneous slurry phase is an oversimplification, although it may be reasonable for smaller particles (d_s < 50 μm) when Re_s < 0.3 and the Stokes law assumption is valid. Krishna and Sie [76] also proposed that the assumption of a pseudo-slurry was valid only for the operation of large columns (i.e., a diameter larger than 0.5 m) at high superficial gas velocities (U_g > 0.2 m·s^{-1}).

Variations in the slurry's apparent physical properties due to the solid presence influence the bubble formation, bubble size, and distribution in the reactor. Krishna et al. [50] observed that the gas voidage of small bubbles significantly decreased with an increase of the solid fraction from 0 to 0.36 due to the enhancement of bubble coalescence. Moreover, empirical correlations of gas holdup and bubble size in the churn-turbulent flow regime were proposed, based on statistics of experimental results [50]. Chilekar et al. [171] proved that the relation of bubble size with slurry concentration was suitable when the solid volume fraction was up to 0.78. The bubble-size distribution has also been shown to be dependent on solid concentration [151].

With an enhanced bubble size due to the solid existence, the gas holdup generally decreases with increasing solid concentration [25,172]. Vandu et al. [173] also indicated that the flow transition velocity decreased and the homogenous regime narrowed with the presence of solids, due to the early formation of large bubbles. Nevertheless, the contrary effects of solids have been found under different operating conditions and solid physical properties. Kelkar et al. [174] showed that solid physical properties, size, and concentration had no significant influence on the gas holdup. Sada et al. [175] argued that the gas holdup decreased with an increased concentration of solids larger than 50 μm, while it increased with the addition of solids smaller than 10 μm. Jamialahmadi and Müller-Steinhagen [176] concluded that the gas holdup increased with wettable solids added but decreased with the addition of non-wettable solids. Mena et al. [177] clarified that the gas holdup first increased with increasing solid concentration and then decreased when the solid volume fraction was higher than 0.03. Correspondingly, the homogeneous regime stabilizes with a solid volume fraction of less than 0.03 and destabilizes when the solid volume fraction is larger than 0.03. Similar dual influences on the liquid velocity have also been demonstrated by Milivojevic et al. [178]. The dual influence of solids on the aforementioned gas holdup and flow transition might result from the steric effect, physical properties, bubble formation and coalescence, and spatial distribution with the addition of solid particles in slurry reactors. Bubble diameter variations have been reported by Rabha et al. [151], who observed large bubbles with the addition of solid particles due to bubble coalescence but found that bubble slugs broke up at high solid volume fractions. In addition, the presence of suspended solids decreases the driving forces for liquid circulation and affects the flow pattern. It is noteworthy that the liquid circulation velocity can be influenced not only by the reactor geometry and superficial gas velocity but also by the flow regime and solids loading [6].

Another noteworthy problem in the three-phase slurry reactor is the obvious axial solid concentration distribution with the highest concentration at the column base, which might result in local overheating. Li et al. [18] found that the axial difference of solid volume fraction can be as high as 76% only 1.4 m away from the column base with 5% solid loading at a superficial gas velocity of 0.03 m·s^{-1} in a two-stage IALR. The non-uniformity of the solid holdup was thought to be caused by advection and circulations of buoyant clusters formed randomly. Murray and Fan [179] argued that the solid axial distribution tended to be more uniform with increasing superficial gas velocity and decreasing particle size in batch and continuous slurry columns. Zhang [180] investigated the axial distribution of the solid holdup in both tapped and cylindrical slurry columns. It was found that the uniformity of the solid axial distribution increased with an increasing superficial gas velocity ranging from 0.02 to 0.28 m·s^{-1} and solid loading varying from 53 to 159 kg·m^{-3}. Meanwhile, decreasing the particle diameter (70–180 μm) and static height (0.6–2.4 m) of the slurry also enhanced the homogeneity of the solid axial distribution. Based

on experimental results, an empirical correlation of the dimensionless Pelect number (*Pe*) was obtained through the least-squares method in order to predict the axial distribution of both monodispersed particles and binary mixtures.

4.4. Other concerns

It has been widely accepted that the hydrodynamics in a slurry reactor is independent of the column size and sparger layout, if *D*, *H*, and *H*/*D* are above certain critical values. Although different critical values have been proposed [26,181,182], the following criteria were recommended for the sake of safe design: ① a diameter greater than 0.2 m; ② an aspect ratio (*H*/*D*) greater than 5; ③ a sparger hole size greater than 1–2 mm [182]. In slurry reactors, the separation problem is aggravated when fine particles are produced by either mechanical or chemical attrition; foam formation is another annoying problem that should be prevented [76].

Xing et al. [134] reported that when the liquid viscosity was less than 10 mPa•s, the influence of liquid viscosity on the bubble breakup rate was negligible, while for a liquid viscosity exceeding 10 mPa•s, the bubble breakup rate decreased with an increase of liquid viscosity. The superficial liquid velocity had little influence on the gas holdup and the k_La [26]. Yang et al. [149] argued that the influence of pressure on the initial bubble diameter was significant under relatively low pressure (below 2.0 MPa), while the influence of pressure on the initial bubble diameter became negligible under high pressure. In addition, high pressure decreased the bubble size and delayed the flow regime transition from the dispersed bubbly flow to the coalesced regime. Wang et al. [26] found that the influence of temperature on the gas–liquid mass transfer was much more prominent than that on the gas voidage, due to a higher liquid diffusivity at high temperatures. Although qualitative conclusions have been drawn, the quantitative results and underlying mechanism involved should be investigated systematically in the future.

5. Computational fluid dynamics modeling

Thanks to rapid developments in mathematics and high-performance computing techniques, CFD has been successfully employed as an efficient tool to investigate the hydrodynamics and transfer properties in gas-agitated slurry reactors [183–185]. The Eulerian–Eulerian model [186], in which all phases are treated as interpenetrating continua, has been widely applied to predict the hydrodynamics in slurry reactors due to its low computational cost. Besides the dispute over turbulence [8], another controversy is the closure of the interphase momentum transfer, which is usually closed by drag, turbulent dispersion, lift, virtual mass, and wall lubrication forces. However, various theoretical and empirical models for these interphase forces have been proposed [187–189]. Thus far, although many researchers have contributed to ensuring the most suitable closure correlations in their simulation cases [190], there is no definite single set of closure models for reliable simulation of the hydrodynamics and mass/heat transfer in multiphase slurry reactors due to their diversified configurations and wide range of operating conditions.

In order to improve the computational accuracy and reduce its expense, different numerical schemes and algorithms have been proposed, as summarized in Table 6 [112,191–201]. Huang et al. [191] simulated the overall gas holdup and mass transfer in an IALR by applying a steady-two-dimensional axisymmetric scheme with an improved decoupling algorithm and specially treated outlet boundary conditions [192]. Oey et al. [193] treated the three-phase system as a pseudo-two-phase one, in which the dispersed solids were included in the liquid slurry phase, by taking into account solid physical properties such as density and viscosity. The solid volume fraction was computed by discretizing the mass-balance equation, in which the solid velocity was the sum of the liquid velocity, slip velocity due to settling, and turbulent dispersion term. It was confirmed that the predicted gas fraction at different gas flow rates aligned with that in the literature. By adopting this pseudo-two-phase model, Wang et al. [194] successfully simulated the local gas holdup and bubble-rise velocity in an EALR.

Constant bubble size with no breakup or coalescence has been commonly employed when calculating the interfacial forces in the balance equations of CFD modeling to reduce the computational cost [202]. However, bubble breakup and the coalescence phenomenon frequently occur in a column, resulting in a wide variation of bubble size and velocity, especially in transition and

Table 6
Numerical investigations of pneumatically agitated slurry reactors.

Refs.	System	Model	Validated parameters	Key points
Huang et al. [191,192]	Gas–liquid IALR	2D steady-two-fluid model	ε_g, k_La	Boundary condition: relative velocity between gas and liquid equals to the bubble terminal velocity
Oey et al. [193]	Gas–liquid–solid IALR	2D pseudo two-fluid model	ε_g, u_l, solid distribution	Solid velocity is the combination of liquid velocity, gravity, and turbulent dispersion
Wang et al. [194]	Gas–liquid–solid EALR	2D pseudo two-fluid model	ε_g, u_l, bubble rise velocity	Modeling the riser section, solid was considered by the liquid–solid physical properties
Chen et al. [195,196]	Gas–liquid bubble column	2D & 3D CFD-PBM	ε_g, u_l, bubble size distribution	Comparison of bubble breakup and coalescence models; increased ten times breakup rate predicted by models
Frank et al. [197]	Gas–liquid	CFD-PBM inhomogeneous MUSIG	ε_g, u_g	Gas phase is divided into *N* inhomogeneous velocity groups with *M* bubble size classes for each group
Yang and Xiao [198]	Gas–liquid bubble column	CFD-PBM	Bubble size distribution	New approach to calculate the coalescence rate through energy-minimization multi-scale concept
Lehr et al. [199]	Gas–liquid bubble column	CFD-PBM	ε_g, u_g, u_l, bubble size distribution	New model for bubble breakup was developed; simplified population balance by utilizing average volume fraction
Ni et al. [200]	Gas–liquid oscillatory baffled column	2D & 3D two-fluid model	Flow pattern	3D simulation of the flow pattern in oscillatory baffled column was first performed
Lestinsky et al. [201]	Gas–liquid IALR	2D two-fluid model	ε_g, u_l	Influence of draft tube geometry and equipping location on hydrodynamics were studied
Moraveji et al. [112]	Gas–liquid packed bed IALR	2D two-fluid model	ε_g, u_l, k_La	Turbulence influences, gas holdup, liquid velocity, and mass transfer were investigated

All the symbols in this table are defined in the Nomenclatures list at the end of this paper.
2D: two-dimensional; 3D: three-dimensional; PBM: population balance model.

turbulent regimes. To remedy this situation, a population balance model (PBM) with a description of bubble coalescence and breakup is incorporated in the CFD scheme to predict the bubble size distribution in the column. The bubble breakup model proposed by Luo and Svendsen [203] and the bubble coalescence model proposed by Prince and Blanch [204] have been verified as being able to reliably describe the bubble distribution in aerated reactors [195,196]. It was first reported by Lo [205] that the hydrodynamics in a bubble column can be well predicted with the CFD-PBM model combined with the developing multi-size group model (MUSIG), in which the bubbles are assumed to have the same motion velocity, for a moderate calculation cost. Frank et al. [197] further developed the inhomogeneous MUSIG, which divided the dispersed phase size into several groups regarding the mass and momentum balance equations. They found that it was sufficient to capture the hydrodynamics in the bubble columns with typically 3–5 groups. Considerable investigations have continually been conducted to obtain a more accurate prediction of the bubble-size distribution. To validate simulation results with experimental data, Chen et al. [196] had to increase the value of the bubble breakage rate by ten times so that the calculated breakage rate from the closure functions could match the experimental data. Bhole et al. [206] suggested that the coalescence kernel should be corrected by a coefficient related to the Stokes number, in which the slip velocity between the liquid and the bubble was considered. Yang and Xiao [198] coupled the energy-minimization multi-scale model with PBM equations to correct the bubble coalescence rate and obtained good agreement with the experimental data.

With numerous studies having developed the mathematical model and discretization scheme, CFD modeling has been widely applied to predict the hydrodynamics and transfer features of gas–liquid and gas–liquid–solid flows, as well as the structural and operational optimization of pneumatically agitated reactors. Lehr et al. [199] successfully predicted the bubble-size distribution and flow regimes in a bubble column using a CFD-PBM model, while treating both large and small bubbles as pseudo-continuous phases in the liquid phase. Lestinsky et al. [201] explored the effects of the geometrical parameters of IALR—that is, the inner diameter, outer diameter, and equipping location of the draft tube—on the liquid circulation velocity and mixing time. Ni et al. [200] performed both two- and three-dimensional unsteady modeling on the flow patterns in an oscillatory baffled column and obtained reasonable agreement with the experimental data using digital particle image velocimetry measurements. Moraveji et al. [112] modeled the intensification of turbulence, hydrodynamics, and mass-transfer properties in a packed bed using a two-fluid turbulent model. They also provided a clear description of the flow patterns, gas holdup distribution, and flow regime transition in the column. Thus, to intensify the hydrodynamics and transfer in a pneumatically agitated reactor, CFD modeling has become an efficient and powerful tool for design, optimization, and scale-up.

6. Conclusions and perspectives

Pneumatically agitated slurry reactors (including bubble columns and ALRs) have a promising future due to their outstanding advantages, which include easy heat removal, excellent temperature control/removal for highly exothermic reactions, low production costs, high interphase mass-transfer rates, and a high online factor for catalyst addition and withdrawal [148,207,208]. Mixing is better in ALRs than in bubble column reactors, due to the intensified well-defined fluid flow. In terms of mass-transfer capability, bubble column reactors are marginally superior to ALRs, due to a relatively higher gas holdup under the same conditions [209,210].

For slurry reactors, challenges such as considerable back-mixing in both the continuous phase and the dispersed gas phase, low volumetric catalyst loading, bubble coalescence, and difficulties in scaling-up remain and should be considered [148]. Meanwhile, the distribution of solids in slurry reactor has been experimentally verified to be non-uniform, especially in the axial direction. This may result in different catalytic reaction rates in different regions, and hot spots and runaways may even occur. It is noteworthy that a margin of temperature between the top and bottom is still observed in slurry reactors [211]. Moreover, the catalyst deactivation rate and attrition may increase with an increase in slurry concentration. Furthermore, foaming, coking, and solid sediment can become severe problems in some applications. Therefore, despite the enormous advantages of pneumatically agitated slurry reactors over multitubular fixed-bed reactors, the slurry reactor technology should be systematically evaluated using an economically and industrially feasible method.

Process intensification is one of the most commonly used methods to improve performance or solve problems in traditional slurry reactors. There are two main categories of process intensification. Methods in the first category involve intensifying the mixing and mass/heat transfer in the slurry reactor and include the use of internals (i.e., tubes, perforated plates, static mixers, and structuring), vibrating excitement, and combination methods for bubble columns, and the use of baffles, perforated plates, static mixers or a packed bed, and mechanical internals for ALRs. It is noteworthy that enhancing the hydrodynamics and transfer in a slurry reactor is highly dependent on the design and operating conditions. Operating a churn-turbulent flow regime at high solid loading and high superficial gas velocity is usually preferred in order to obtain a high space–time yield. To remove the high exothermic heat of reaction efficiently, large amounts of equipment for heat removal are very desirable, and the hydrodynamics in the slurry may be correspondingly affected to a significant degree. The second category involves combining the mixing and the solid–liquid separation within the same slurry reactor in order to realize continuous production and reduce cost. The new technology of integrating directional flow in IALRs with low-cost solid–liquid separation through a hydrocyclone is one of the most competitive methods. For this novel technology, a compact and efficient hydrocyclone with a low pressure drop is one of the decisive factors [212]. It should be noted that the separation of very fine particles from liquid products usually requires multiple separation methods.

Although great endeavors have been made in this field, it remains difficult to design and scale-up industrial slurry reactors due to limited experimental information on hydrodynamics and mass transfer over a wide range of operating conditions. CFD has been verified as a powerful tool for investigating the hydrodynamics and transfer properties in pneumatically agitated slurry reactors. The CFD-PBM model is regarded as the most promising model for numerical simulations. However, it has been widely accepted that current simulations cannot predict the bimodal bubble-size distribution in a heterogeneous regime, and different bubble coalescence and breakup models may even give different bubble-size distributions [8,134]. Therefore, CFD models should be developed and validated against experimental data. Otherwise, they will be dangerous, and the predicted results will be more art than science [213].

Nomenclatures

Symbols

a	mass-transfer interfacial area (m^2)
A_d	downcomer cross-sectional area (m^2)
A_D	column cross-sectional area (m^2)
A_p	exciter disk surface area (m^2)
A_r	riser cross-sectional area (m^2)
A_0	amplitude of imposed liquid pulsation (cm)
b_1, b_2	model constant
c_1, c_2, c_3	model constant
d	diameter or sieve pore diameter (mm)
d_{32}	bubble Sauter diameter (mm)
$-d\sigma/dC$	surface tension gradient ($N{\cdot}m^2{\cdot}mol^{-1}$)
d_0	sieve pore diameter (mm)
D	internal diameter of the column (mm)
$D_{s,l}$	liquid axial dispersion coefficient
D_0	the diffusivity of a reference fluid ($cm^2{\cdot}s^{-1}$)
E	axial dispersion coefficient
F	vibration frequency (Hz)
f_i^*	specific frequency of pulsations (Hz)
g	acceleration due to gravity ($cm{\cdot}s^{-2}$)
H	height (mm)
h_p	packing height (m)
k	mass transfer coefficient ($m{\cdot}s^{-1}$)
k_La	volumetric mass-transfer coefficient (s^{-1})
L	length of the circulation loop (m)
N	number
n	numbers of sieve plates
P	power input (W)
P_A	energy dissipation rate for aeration ($W{\cdot}m^{-3}$)
P_m	power input per unit mass ($W{\cdot}kg^{-1}$)
P_p	energy dissipation rate for mechanical agitation ($W{\cdot}m^{-3}$)
P_0	pressure at top interface (Pa)
p_1, p_2, p_3, p_4, p_5	model parameters
P/V	power density ($W{\cdot}m^{-3}$)
Q	volumetric gas flow rate ($mL{\cdot}min^{-1}$)
S	space distance (mm)
T	temperature (K)
U	superficial velocity ($m{\cdot}s^{-1}$)
u	velocity ($m{\cdot}s^{-1}$)
U_{gsr}	total riser superficial gas velocity ($m{\cdot}s^{-1}$)
U_{gsd}	downcomer superficial gas velocity ($m{\cdot}s^{-1}$)
U_{LR}	liquid riser velocity ($m{\cdot}s^{-1}$)
U_0	orifice speed ($m{\cdot}s^{-1}$)
X_p	amplitude of disk vibrations (m)
x_0	oscillatory amplitude from center to peak (m)

Greek symbols

α	free area ratio of the sieve plates
θ	helical angle (°)
λ	vibration amplitude (mm)
λ_1	model constant
μ	dynamic viscosity (Pa·s)
μ_{eff}	effective viscosity (Pa·s)
μ_{slurry}	apparent viscosity of the slurry (Pa·s)
ν	kinematic liquid viscosity ($m^2{\cdot}s^{-1}$)
ν_0	the kinematic viscosity of a reference fluid ($m^2{\cdot}s^{-1}$)
ε	volume fraction
ρ	density ($kg{\cdot}m^{-3}$)
σ	surface tension ($N{\cdot}m^{-1}$)
ϕ	packing porosity
ϕ_s	solid volume fraction
$\phi_{s,max}$	maximum solid volume fraction
Ω	frequency ($rad{\cdot}s^{-1}$)1

Subscripts

b	bubble column
g	gas
l	liquid
o	orifice
p	sieve plates
s	solid

Dimensionless numbers

Bj	Bjerknes number, $Bj = \frac{1}{2}\rho H A_0^2 \omega^4/(gP_0)$
Bo	Bodenstein number, $Bo = U_{LR}L/D$
Fr	Froude number, $Fr = U_g/\sqrt{gD}$
Ga	Galileo number, $Ga = \rho g L^3/\mu^2$
Pe	Pelect number, $Pe = UL/E$
Re	Reynolds number, $Re = DU\rho/\mu$
Re_o	oscillatory Reynolds number, $Re_0 = \rho\omega x_0 d/\mu$
Re'_0	modified oscillatory Reynolds number, $Re'_0 = \left(\frac{2\pi f \lambda \rho}{\mu}\right)\left(\frac{D}{\sqrt{n}}\right)\sqrt{\frac{1-a}{a^2}}$
Sh	Sherwood number, $Sh = Lk_1/D_{s,l}$
Str	Strouhal number, $Str = d/(4\pi\lambda)$
St'	modified Strouhal number, $St' = \frac{D}{4\pi\lambda}\frac{1}{\sqrt{n}}$
Sc	Schmidt number, $Sc = \mu/(\rho E)$

Acknowledgements

This work was supported by the National Key Research and Development Program of China (2016YFB0301701), the National Natural Science Foundation of China (21808234, 21878318, and 21938009), the DNL Cooperation Fund, Chinese Academy of Sciences (CAS) (DNL201902), the Strategic Priority Research Program of the CAS (XDA21060400), the QIBEBT and Dalian National Laboratory for Clean Energy of the CAS (QIBEBT ZZBS201803 and QIBEBT I201907), and the CAS Key Technology Talent Program.

Compliance with ethics guidelines

Shujun Geng, Zai-Sha Mao, Qingshan Huang, and Chao Yang declare that they have no conflict of interest or financial conflicts to disclose.

References

[1] Al-Qodah Z, Lafi W. Modeling of antibiotics production in magneto three-phase airlift fermenter. Biochem Eng J 2001;7(1):7–16.

[2] Van Benthum WAJ, Van der Lans RGJM, Van Loosdrecht MCM, Heijnen JJ. The biofilm airlift suspension extension reactor—II: three-phase hydrodynamics. Chem Eng Sci 2000;55(3):699–711.

[3] Huang Q, Liu T, Yang J, Yao L, Gao L. Evaluation of radiative transfer using the finite volume method in cylindrical photoreactors. Chem Eng Sci 2011;66(17):3930–40.

[4] Huang Q, Yao L, Liu T, Yang J. Simulation of the light evolution in an annular photobioreactor for the cultivation of *Porphyridium cruentum*. Chem Eng Sci 2012;84:718–26.

[5] Huang Q, Zhang W, Yang C. Modeling transport phenomena and reactions in a pilot slurry airlift loop reactor for direct coal liquefaction. Chem Eng Sci 2015;135:441–51.

[6] Jin B, Yin P, Lant P. Hydrodynamics and mass transfer coefficient in three-phase airlift reactors containing activated sludge. Chem Eng Process 2006;45(7):608–17.

[7] Guo X, Yao L, Huang Q. Aeration and mass transfer optimization in a rectangular airlift loop photobioreactor for the production of microalgae. Bioresour Technol 2015;190:189–95.
[8] Yang C, Mao ZS. Numerical simulation of multiphase reactors with continuous liquid phase. London: Elsevier Academic Press; 2014.
[9] Huang Q, Jiang F, Wang L, Yang C. Design of photobioreactors for mass cultivation of photosynthetic organisms. Engineering 2017;3(3):318–29.
[10] Russell AB, Thomas CR, Lilly MD. The influence of vessel height and top-section size on the hydrodynamic characteristics of airlift fermentors. Biotechnol Bioeng 1994;43(1):69–76.
[11] Choi KH, Lee WK. Circulation liquid velocity, gas holdup and volumetric oxygen transfer coefficient in external-loop airlift reactors. J Chem Technol Biotechnol 1993;56(1):51–8.
[12] Vial C, Lainé R, Poncin S, Midoux N, Wild G. Influence of gas distribution and regime transitions on liquid velocity and turbulence in a 3-D bubble column. Chem Eng Sci 2001;56(3):1085–93.
[13] Huang Q, Yang C, Yu G, Mao ZS. 3-D simulations of an internal airlift loop reactor using a steady two-fluid model. Chem Eng Technol 2007;30(7):870–9.
[14] Dhaouadi H, Poncin S, Hornut JM, Wild G. Solid effects on hydrodynamics and heat transfer in an external loop airlift reactor. Chem Eng Sci 2006;61(4):1300–11.
[15] Heijnen JJ, Hols J, Van der Lans RGJM, Van Leeuwen HLJM, Mulder A, Weltevrede R. A simple hydrodynamic model for the liquid circulation velocity in a full-scale two- and three-phase internal airlift reactor operating in the gas recirculation regime. Chem Eng Sci 1997;52(15):2527–40.
[16] Kundakovic L, Vunjak-Novakovic G. A fluid dynamic-model of the draft tube gas–liquid–solid fluidized bed. Chem Eng Sci 1995;50(23):3763–75.
[17] Lukić NL, Sijacki IM, Kojic PS, Popovic SS, Tekic MN, Petrovic DL. Enhanced mass transfer in a novel external-loop airlift reactor with self-agitated impellers. Biochem Eng J 2017;118:53–63.
[18] Li D, Guo K, Li J, Huang Y, Zhou J, Liu H, et al. Hydrodynamics and bubble behaviour in a three-phase two-stage internal loop airlift reactor. Chin J Chem Eng 2018;26(6):1359–69.
[19] Chen J, Li F, Degaleesan S, Gupta P, Al-Dahhan MH, Dudukovic HMP, et al. Fluid dynamic parameters in bubble columns with internals. Chem Eng Sci 1999;54(13–14):2187–97.
[20] Dreher AJ, Krishna R. Liquid-phase backmixing in bubble columns, structured by introduction of partition plates. Catal Today 2001;69(1–4):165–70.
[21] Pangarkar K, Schildhauer TJ, Van Ommen JR, Nijenhuis J, Moulijn JA, Kapteijn F. Experimental and numerical comparison of structured packings with a randomly packed bed reactor for Fischer–Tropsch synthesis. Catal Today 2009;147(Suppl):S2–9.
[22] Guettel R, Kunz U, Turek T. Reactors for Fischer–Tropsch synthesis. Chem Eng Technol 2008;31(5):746–54.
[23] Jager B, Espinoza R. Advances in low-temperature Fischer–Tropsch synthesis. Catal Today 1995;23(1):17–28.
[24] Savchenko VI, Dorokhov VG, Makaryan IA, Sedov IV, Arutyunov VS. Slurry reactor system with inertial separation for Fischer–Tropsch synthesis and other three-phase hydrogenation processes. Can J Chem Eng 2016;94(3):518–23.
[25] Yang T, Geng S, Yang C, Huang Q. Hydrodynamics and mass transfer in an internal airlift slurry reactor for process intensification. Chem Eng Sci 2018;184:126–33.
[26] Wang T, Wang J, Jin Y. Slurry reactors for gas-to-liquid processes: a review. Ind Eng Chem Res 2007;46(18):5824–47.
[27] Cozma P, Gavrilescu M. Airlift reactors: hydrodynamics, mass transfer and applications in environmental remediation. Environ Eng Manag J 2010;9(5):681–702.
[28] Cozma P, Gavrilescu M. Airlift reactors: applications in wastewater treatment. Environ Eng Manag J 2012;11(8):1505–15.
[29] Yang GQ, Fan LS. Axial liquid mixing in high-pressure bubble columns. AIChE J 2003;49(8):1995–2008.
[30] Yadav A, Kushwaha A, Roy S. An algorithm for estimating radial gas holdup profiles in bubble columns from chordal densitometry measurements. Can J Chem Eng 2016;94(3):524–9.
[31] Shah YT, Kelkar BG, Godbole SP, Deckwer WD. Design parameters estimations for bubble column reactors. AIChE J 1982;28(3):353–79.
[32] Wu Y, Gidaspow D. Hydrodynamic simulation of methanol synthesis in gas–liquid slurry bubble column reactors. Chem Eng Sci 2000;55(3):573–87.
[33] Gupta P, Al-Dahhan MH, Dudukovic MP, Toseland BA. Comparison of single- and two-bubble class gas–liquid recirculation models—application to pilot-plant radioactive tracer studies during methanol synthesis. Chem Eng Sci 2001;56(3):1117–25.
[34] Youssef AA, Al-Dahhan MH. Impact of internals on the gas holdup and bubble properties of a bubble column. Ind Eng Chem Res 2009;48(17):8007–13.
[35] Kagumba M, Al-Dahhan MH. Impact of internals size and configuration on bubble dynamics in bubble columns for alternative clean fuels production. Ind Eng Chem Res 2015;54(4):1359–72.
[36] Forret A, Schweitzer JM, Gauthier T, Krishna R, Schweich D. Liquid dispersion in large diameter bubble columns, with and without internals. Can J Chem Eng 2003;81(3–4):360–6.
[37] Pradhan AK, Parichha RK, De P. Gas hold-up in non-Newtonian solutions in a bubble column with internals. Can J Chem Eng 1993;71(3):468–71.
[38] Saxena SC, Rao NS, Thimmapuram PR. Gas phase holdup in slurry bubble columns for two- and three-phase systems. Chem Eng J 1992;49(3):151–9.
[39] Fair JR, Lambright AJ, Andersen JW. Heat transfer and gas holdup in a sparged contactor. Ind Eng Chem Process Des Dev 1962;1(1):33–6.
[40] Palaskar SN, De JK, Pandit AB. Liquid phase RTD studies in sectionalized bubble column. Chem Eng Technol 2000;23(1):61–9.
[41] Rabha S, Schubert M, Grugel F, Banowski M, Hampel U. Visualization and quantitative analysis of dispersive mixing by a helical static mixer in upward co-current gas–liquid flow. Chem Eng J 2015;262:527–40.
[42] Gaspillo PAD, Goto S. Mass transfer in bubble slurry column with static mixer in draft tube. J Chem Eng of Jpn 1991;24(5):680–2.
[43] Urseanu MI, Ellenberger J, Krishna R. A structured catalytic bubble column reactor: hydrodynamics and mixing studies. Catal Today 2001;69(1–4):105–13.
[44] Khamadieva R, Böhm U. Mass transfer to the wall of a packed and unpacked bubble column operating with Newtonian and non-Newtonian liquids. Chem Eng J 2006;116(2):105–13.
[45] Sultan AJ, Sabri LS, Al-Dahhan MH. Influence of the size of heat exchanging internals on the gas holdup distribution in a bubble column using gamma-ray computed tomography. Chem Eng Sci 2018;186:1–25.
[46] Al Mesfer MK, Sultan AJ, Al-Dahhan MH. Impacts of dense heat exchanging internals on gas holdup cross-sectional distributions and profiles of bubble column using gamma ray computed tomography (CT) for FT synthesis. Chem Eng J 2016;300:317–33.
[47] Chen BH, Yang NS, Mcmillan AF. Gas holdup and pressure drop for air–water flow through plate bubble columns. Can J Chem Eng 1986;64(3):387–92.
[48] Magnussen P, Schumacher V, Rotermund GW, Hafner F. Residence time behavior of liquid-phase in bubble columns of larger diameter. Chem Ing Tech 1978;50(10):811.
[49] Krishna R, Urseanu MI, Van Baten JM, Ellenberger J. Liquid phase dispersion in bubble columns operating in the churn-turbulent flow regime. Chem Eng J 2000;78(1):43–51.
[50] Krishna R, Urseanu MI, Van Baten JM, Ellenberger J. Rise velocity of a swarm of large gas bubbles in liquids. Chem Eng Sci 1999;54(2):171–83.
[51] Chen B. Effects of liquid flow on axial mixing liquid in a bubble column. Can J Chem Eng 1972;50(3):436–8.
[52] Deckwer W, Graeser U, Langemann H, Serpemen Y. Zones of different mixing in the liquid phase of bubble columns. Chem Eng Sci 1973;28(5):1223–5.
[53] Thakur RK, Vial C, Nigam KDP, Nauman EB, Djelveh G. Static mixers in the process industries—a review. Chem Eng Res Des 2003;81(7):787–826.
[54] Fan LT, Hsu HH, Wang KB. Mass-transfer coefficient and pressure-drop data of two-phase oxygen–water flow in bubble column packed with static mixers. J Chem Eng Data 1975;20(1):26–8.
[55] Wang KB, Fan LT. Mass transfer in bubble columns packed with motionless mixers. Chem Eng Sci 1978;33(7):945–52.
[56] Hooshyar N, Vervloet D, Kapteijn F, Hamersma PJ, Mudde RF, Van Ommen JR. Intensifying the Fischer–Tropsch synthesis by reactor structuring—a model study. Chem Eng J 2012;207–208:865–70.
[57] Spiegel L, Meier W. Distillation columns with structured packings in the next decade. Chem Eng Res Des 2003;81(1):39–47.
[58] Horiuchi J, Tabata K, Kanno T, Kobayashi M. Continuous acetic acid production by a packed bed bioreactor employing charcoal pellets derived from waste mushroom medium. J Biosci Bioeng 2000;89(2):126–30.
[59] Pangarkar K, Schildhauer TJ, Van Ommen JR, Nijenhuis J, Kapteijn F, Moulijn JA. Structured packings for multiphase catalytic reactors. Ind Eng Chem Res 2008;47(10):3720–51.
[60] Nijhuis TA, Kreutzer MT, Romijn ACJ, Kapteijn F, Moulijn JA. Monolithic catalysts as efficient three-phase reactors. Chem Eng Sci 2001;56(3):823–9.
[61] Pangarkar K, Schildhauer TJ, Van Ommen JR, Nijenhuis J, Moulijn JA, Kapteijn F. Heat transport in structured packings with co-current downflow of gas and liquid. Chem Eng Sci 2010;65(1):420–6.
[62] Schildhauer TJ, Pangarkar K, Van Ommen JR, Nijenhuis J, Moulijn JA, Kapteijn F. Heat transport in structured packings with two-phase co-current downflow. Chem Eng J 2012;185–186:250–66.
[63] Baird MHI. Vibrations and pulsations-bane or blessing. Br Chem Eng 1966;11(1):20–5.
[64] Ellenberger J, Krishna R. Improving mass transfer in gas–liquid dispersions by vibration excitement. Chem Eng Sci 2002;57(22–23):4809–15.
[65] Ellenberger J, Krishna R. Shaken, not stirred, bubble column reactors: enhancement of mass transfer by vibration excitement. Chem Eng Sci 2003;58(3–6):705–10.
[66] Ellenberger J, Van Baten JM, Krishna R. Intensification of bubble columns by vibration excitement. Catal Today 2003;79–80:181–8.
[67] Ellenberger J, Krishna R. Intensification of slurry bubble columns by vibration excitement. Can J Chem Eng 2003;81(3–4):655–9.
[68] Knopf FC, Ma J, Rice RG, Nikitopoulos D. Pulsing to improve bubble column performance: I. low gas rates. AIChE J 2006;52(3):1103–15.
[69] Knopf FC, Waghmare Y, Ma J, Rice RG. Pulsing to improve bubble column performance: II. jetting gas rates. AIChE J 2006;52(3):1116–26.
[70] Waghmare YG, Rice RG, Knopf FC. Mass transfer in a viscous bubble column with forced oscillations. Ind Eng Chem Res 2008;47(15):5386–94.
[71] Budzyński P, Dziubiński M. Intensification of bubble column performance by introduction pulsation of liquid. Chem Eng Process 2014;78:44–57.
[72] Ellenberger J, Van Baten JM, Krishna R. Exploiting the Bjerknes force in bubble column reactors. Chem Eng Sci 2005;60(22):5962–70.
[73] Budzyński P, Gwiazda A, Dziubiński M. Intensification of mass transfer in a pulsed bubble column. Chem Eng Process 2017;112:18–30.

[74] Hinze JO. Fundamentals of the hydrodynamic mechanism of splitting in dispersion process. AIChE J 1955;1(3):289–95.
[75] Buchanan RH, Jameson G, Oedjoe D. Cycle migration of bubbles in vertically vibrating liquid columns. Ind Eng Chem Fundam 1962;1(2):82–6.
[76] Krishna R, Sie ST. Design and scale-up of the Fischer–Tropsch bubble column slurry reactor. Fuel Process Technol 2000;64(1–3):73–105.
[77] Maretto C, Krishna R. Design and optimisation of a multi-stage bubble column slurry reactor for Fischer–Tropsch synthesis. Catal Today 2001;66(2–4):241–8.
[78] Lucas MS, Reis NM, Li PG. Intensification of ozonation processes in a novel, compact, multi-orifice oscillatory baffled column. Chem Eng J 2016;296:335–9.
[79] Pereira FM, Sousa DZ, Alves MM, Mackley MR, Reis NM. CO_2 dissolution and design aspects of a multiorifice oscillatory baffled column. Ind Eng Chem Res 2014;53(44):17303–16.
[80] Ahmed SMR, Phan AN, Harvey AP. Mass transfer enhancement as a function of oscillatory baffled reactor design. Chem Eng Process 2018;130:229–39.
[81] Ni X, Gao S. Scale-up correlation for mass transfer coefficients in pulsed baffled reactors. Chem Eng J Biochem Eng J 1996;63(3):157–66.
[82] Oliveira MSN, Fitch AW, Ni X. A study of bubble velocity and bubble residence time in a gassed oscillatory baffled column: effect of oscillation frequency. Chem Eng Res Des 2003;81(2):233–42.
[83] Oliveira MSN, Fitch AW, Ni XW. A study of velocity and residence time of single bubbles in a gassed oscillatory baffled column: effect of oscillation amplitude. J Chem Technol Biotechnol 2003;78(2–3):220–6.
[84] Oliveira MSN, Ni X. Gas hold-up and bubble diameters in a gassed oscillatory baffled column. Chem Eng Sci 2001;56(21–22):6143–8.
[85] Smith KB, Mackley MR. An experimental investigation into the scale-up of oscillatory flow mixing in baffled tubes. Chem Eng Res Des 2006;84(11):1001–11.
[86] Laso M, de Brito MH, Bomio P, von Stockar U. Liquid-side mass transfer characteristics of a structured packing. Chem Eng J Biochem Eng J 1995;58(3):251–8.
[87] Huang Q, Zhang W, Yang C, Mao ZS. Characteristics of multiphase flow, mixing and transport phenomena in airlift loop reactor. CIESC J 2014;65(7):2465–73.
[88] Tao J, Huang J, Xiao H, Yang C, Huang Q. Influences of interstage height and superficial gas velocity in multistage internal airlift loop reactor on performance of mixing and mass transfer. CIESC J 2018;69(7):2878–89.
[89] Gluz MD, Merchuk JC. Modified airlift reactors: the helical flow promoters. Chem Eng Sci 1996;51(11):2915–20.
[90] Schlötelburg C, Popovic M, Gluz M, Merchuk JC. Characterization of an airlift reactor with helical flow promoters. Can J Chem Eng 1999;77(5):804–10.
[91] Räsänen M, Eerikäinen T, Ojamo H. Characterization and hydrodynamics of a novel helix airlift reactor. Chem Eng Process 2016;108:44–57.
[92] Luo L, Yuan J, Xie P, Sun J, Guo W. Hydrodynamics and mass transfer characteristics in an internal loop airlift reactor with sieve plates. Chem Eng Res Des 2013;91(12):2377–88.
[93] Zheng Z, Chen Y, Zhan X, Gao M, Wang Z. Mass transfer intensification in a novel airlift reactor assembly with helical sieve plates. Chem Eng J 2018;342:61–70.
[94] Chisti Y, Kasper M, Moo-Young M. Mass transfer in external-loop airlift bioreactors using static mixers. Can J Chem Eng 1990;68(1):45–50.
[95] Goto S, Gaspillo PD. The effect of static mixer on mass transfer in draft tube bubble column and in external loop column. Chem Eng Sci 1992;47(13–14):3533–9.
[96] Lu XP, Wang YR, Shi J. Transfer characteristics in mechanically stirred airlift loop reactors with or without static mixers. Chin J Chem Eng 2000;8(3):208–11.
[97] Meng AX, Hill GA, Dalai AK. Hydrodynamic characteristics in an external loop airlift bioreactor containing a spinning sparger and a packed bed. Ind Eng Chem Res 2002;41(9):2124–8.
[98] Wu XX, Merchuk JC. Measurement of fluid flow in the downcomer of an internal loop airlift reactor using an optical trajectory-tracking system. Chem Eng Sci 2003;58(8):1599–614.
[99] Pi K, Huang L, Li Z, Gao L, Gerson AR. Oxygen mass transfer characteristics in an internal-loop airlift reactor with preset trumpet-shaped riser. Asia-Pac J Chem Eng 2014;9(6):834–44.
[100] Krichnavaruk S, Pavasant P. Analysis of gas–liquid mass transfer in an airlift contactor with perforated plates. Chem Eng J 2002;89(1–3):203–11.
[101] Vorapongsathorn T, Wongsuchoto P, Pavasant P. Performance of airlift contactors with baffles. Chem Eng J 2001;84(3):551–6.
[102] Zhang TW, Wang JF, Wang TF, Lin J, Jin Y. Effect of internal on the hydrodynamics in external-loop airlift reactors. Chem Eng Process 2005;44(1):81–7.
[103] Yu W, Wang T, Song F, Wang Z. Investigation of the gas layer height in a multistage internal-loop airlift reactor. Ind Eng Chem Res 2009;48(20):9278–85.
[104] Yu W, Wang T, Liu M, Song F. Investigation of operation regimes in a multistage internal-loop airlift reactor. Ind Eng Chem Res 2010;49(22):11752–9.
[105] Hsu CH, Chu YF, Argin-Soysal S, Hahm TS, Lo YM. Effects of surface characteristics and xanthan polymers on the immobilization of *Xanthomonas campestris* to fibrous matrices. J Food Sci 2004;69(9):E441–8.
[106] Kilonzo P, Margaritis A, Bergougnou M. Airlift-driven fibrous-bed bioreactor for continuous production of glucoamylase using immobilized recombinant yeast cells. J Biotechnol 2009;143(1):60–8.
[107] Nikakhtari H, Hill GA. Enhanced oxygen mass transfer in an external loop airlift bioreactor using a packed bed. Ind Eng Chem Res 2005;44(4):1067–72.
[108] Nikakhtari H, Hill GA. Volatile organic chemical mass transfer in an external loop airlift bioreactor with a packed bed. Ind Eng Chem Res 2005;44(24):9299–306.
[109] Nikakhtari H, Hill GA. Continuous bioremediation of phenol-polluted air in an external loop airlift bioreactor with a packed bed. J Chem Technol Biotechnol 2006;81(6):1029–38.
[110] Hamood-ur-Rehman M, Dahman Y, Ein-Mozaffari F. Investigation of mixing characteristics in a packed-bed external loop airlift bioreactor using tomography images. Chem Eng J 2012;213:50–61.
[111] Hamood-ur-Rehman M, Ein-Mozaffari F, Dahman Y. Dynamic and local gas holdup studies in external loop recirculating airlift reactor with two rolls of fiberglass packing using electrical resistance tomography. J Chem Technol Biotechnol 2013;88(5):887–96.
[112] Moraveji MK, Sajjadi B, Jafarkhani M, Davarnejad R. Experimental investigation and CFD simulation of turbulence effect on hydrodynamic and mass transfer in a packed bed airlift internal loop reactor. Int Commun Heat Mass Transfer 2011;38(4):518–24.
[113] Kilonzo PM, Margaritis A, Bergougnou MA. Hydrodynamics and mass transfer characteristics in an inverse internal loop airlift-driven fibrous-bed bioreactor. Chem Eng J 2010;157(1):146–60.
[114] Nikakhtari H, Hill GA. Hydrodynamic and oxygen mass transfer in an external loop airlift bioreactor with a packed bed. Biochem Eng J 2005;27(2):138–45.
[115] Tekic MN, Sijacki IM, Tokic MS, Kojic PS, Petrovic DL, Lukic NL, et al. Hydrodynamics of self-agitated draft tube airlift reactor. Chem Ind Chem Eng Q 2014;20(1):59–69.
[116] Lukić NL, Šijački IM, Kojić PS, Popović SS, Tekić MN, Petrović DL. Enhanced hydrodynamics in a novel external-loop airlift reactor with self-agitated impellers. J Taiwan Inst Chem Eng 2016;68:40–50.
[117] Benham CB, Yakobson DL, Bohn MS, inventors; Rentech Inc., Res USA LLC, assignees. Catalyst/wax separation device for slurry Fischer–Tropsch reactor. United Sates patent US 6068760A. 2000 May 30.
[118] Pashkova A, Svajda K, Dittmeyer R. Direct synthesis of hydrogen peroxide in a catalytic membrane contactor. Chem Eng J 2008;139(1):165–71.
[119] Qi Y, Chen M, Liang S, Yang W, Zhao J. Micro-patterns of Au@SiO_2 core–shell nanoparticles formed by electrostatic interactions. Appl Surf Sci 2008;254(6):1684–90.
[120] Liu H, Wang Y, Han T, Huang Q. Influence of vortex finder configurations on separation of fine particles. CIESC J 2017;68(5):1921–31.
[121] Liu H, Han T, Wang Y, Huang Q. Influence of new outlet configurations with baffle on hydrocycloneon separation performance. CIESC J 2018;69(5):2081–8.
[122] Rytter E, Lian P, Myrstad T, Roterud PT, Solbakken A, inventors; Statoil ASA, assignee. Method of conducting catalytic converter multi-phase reaction. United States patent US 5422375A 1995 Jun 6.
[123] Jager B, Steynberg AP, Inga JR, Kelfkens RC, Smith MA, Malherbe FEJ, inventors; Sasol Chemical Industries (Pty) Ltd., Sasol Technology Pty Ltd., assignees. Process for producing liquid and, optionally, gaseous products from gaseous reactants. United States patent US 5599849A. 1997 Feb 4.
[124] Anderson JH, inventor; Texaco Inc., assignee. Internal filter for Fischer–Tropsch catalyst/wax separation. United States patent US 6652760B2 2003 Nov 25.
[125] Clerici GCE, Belmonte G, invemtors;. ENI SpA, Institut Francais du Petrole, EniTechnologie SpA, assignees. Process for the production in continuous of hydrocarbons from synthesis gas in slurry reactions and for the separation of the liquid phase produced from the solid phase. United Kingdom patent GB 2403433B 2004 Jun 11.
[126] White CM, Quiring MS, Jensen KL, Hickey RF, Gillham LD, inventors; US Department of Energy, assignee. Separation of catalyst from Fischer–Tropsch slurry. United States patent US 5827903A. 1998 Oct 27.
[127] Hu L, Tang X, Zhang Z, Zhu Z, inventors; Sinopec, Sinopec Research Institute of Petroleum Processing, assignees. [A slurry bed reaction and separation equipment]. China patent CN 202823321U. 2013 Mar 27. Chinese.
[128] Hu L, Tang X, Zhang Z, Zhu Z, inventors; Sinopec, Sinopec Research Institute of Petroleum Processing, assignees. [A slurry airlift loop reactor and continuous separation equipment]. China patent CN 203018065U. 2013 Jun 26. Chinese.
[129] Papari S, Kazemeini M, Fattahi M. Modelling-based optimisation of the direct synthesis of dimethyl ether from syngas in a commercial slurry reactor. Chin J Chem Eng 2013;21(6):611–21.
[130] Thorat BN, Joshi JB. Regime transition in bubble columns: experimental and predictions. Exp Therm Fluid Sci 2004;28(5):423–30.
[131] Nabipoor Hassankiadeh M, Haghtalab A. Product distribution of Fischer–Tropsch synthesis in a slurry bubble column reactor based on Langmuir–Freundlich isotherm. Chem Eng Commun 2013;200(9):1170–86.
[132] Van der Laan GP, Beenackers AACM, Krishna R. Multicomponent reaction engineering model for Fe-catalyzed Fischer–Tropsch synthesis in commercial scale slurry bubble column reactors. Chem Eng Sci 1999;54(21):5013–9.
[133] Forret A, Schweitzer JM, Gauthier T, Krishna R, Schweich D. Scale up of slurry bubble reactors. Oil Gas Sci Technol 2006;61(3):443–58.
[134] Xing C, Wang T, Wang J. Experimental study and numerical simulation with a coupled CFD-PBM model of the effect of liquid viscosity in a bubble column. Chem Eng Sci 2013;95:313–22.

[135] Van Baten JM, Krishna R. Eulerian simulation strategy for scaling up a bubble column slurry reactor for Fischer–Tropsch synthesis. Ind Eng Chem Res 2004;43(16):4483–93.
[136] Snape JB, Fialova M, Zahradnik J, Thomas NH. Hydrodynamic studies in an external loop airlift reactor containing aqueous electrolyte and sugar solutions. Chem Eng Sci 1992;47(13–14):3387–94.
[137] Luo L, Liu F, Xu Y, Yuan J. Hydrodynamics and mass transfer characteristics in an internal loop airlift reactor with different spargers. Chem Eng J 2011;175:494–504.
[138] Xiao H, Geng S, Chen A, Yang C, Gao F, He T, et al. Bubble formation in continuous liquid phase under industrial jetting conditions. Chem Eng Sci 2019;200:214–24.
[139] Lin J, Han M, Wang T, Zhang T, Wang J, Jin Y. Influence of the gas distributor on the local hydrodynamic behavior of an external loop airlift reactor. Chem Eng J 2004;102(1):51–9.
[140] Wei C, Wu B, Li G, Chen K, Jiang M, Ouyang P. Comparison of the hydrodynamics and mass transfer characteristics in internal-loop airlift bioreactors utilizing either a novel membrane-tube sparger or perforated plate sparger. Bioprocess Biosyst Eng 2014;37(11):2289–304.
[141] Hooshyar N, Hamersma PJ, Mudde RF, Van Ommen JR. Intensified operation of slurry bubble columns using structured gas injection. Can J Chem Eng 2010;88(4):533–42.
[142] Hooshyar N, Hamersma PJ, Mudde RF, Van Ommen JR. Gas fraction and bubble dynamics in structured slurry bubble columns. Ind Eng Chem Res 2010;49(21):10689–97.
[143] Vial C, Camarasa E, Poncin S, Wild G, Midoux N, Bouillard J. Study of hydrodynamic behaviour in bubble columns and external loop airlift reactors through analysis of pressure fluctuations. Chem Eng Sci 2000;55 (15):2957–73.
[144] Cao C, Dong S, Geng Q, Guo Q. Hydrodynamics and axial dispersion in a gas–liquid–(solid) EL-ALR with different sparger designs. Ind Eng Chem Res 2008;47(11):4008–17.
[145] Han L, Al-Dahhan MH. Gas–liquid mass transfer in a high pressure bubble column reactor with different sparger designs. Chem Eng Sci 2007;62(1–2):131–9.
[146] Michele V, Hempel DC. Liquid flow and phase holdup-measurement and CFD modeling for two- and three-phase bubble columns. Chem Eng Sci 2002;57 (11):1899–908.
[147] Li H, Prakash A. Heat transfer and hydrodynamics in a three-phase slurry bubble column. Ind Eng Chem Res 1997;36(11):4688–94.
[148] Gandhi B, Prakash A, Bergougnou MA. Hydrodynamic behavior of slurry bubble column at high solids concentrations. Powder Technol 1999;103 (2):80–94.
[149] Yang GQ, Du B, Fan LS. Bubble formation and dynamics in gas–liquid–solid fluidization—a review. Chem Eng Sci 2007;62(1–2):2–27.
[150] Maretto C, Krishna R. Modelling of a bubble column slurry reactor for Fischer–Tropsch synthesis. Catal Today 1999;52(2–3):279–89.
[151] Rabha S, Schubert M, Wagner M, Lucas D, Hampel U. Bubble size and radial gas hold-up distributions in a slurry bubble column using ultrafast electron beam X-ray tomography. AIChE J 2013;59(5):1709–22.
[152] Wang TF, Wang JF, Yang WG, Jin Y. Experimental study on bubble behavior in gas–liquid–solid three-phase circulating fluidized beds. Powder Technol 2003;137(1–2):83–90.
[153] Abdel-Aziz MH, Nirdosh I, Sedahmed GH. Liquid–solid mass and heat transfer behavior of a concentric tube airlift reactor. Int J Heat Mass Transfer 2013;58 (1–2):735–9.
[154] Guth E, Simha R. Explorations of the viscosity of suspensions and solutions 3. The viscosity of sphere suspensions (the calculation of wall influence and the exchange effect in viscosity as well as in rotating spheres). Kolloid-Zeitschrift 1936;74(3):266–75. German.
[155] Vand V. Viscosity of solutions and suspensions. I. Theory. J Phys Colloid Chem 1948;52(2):277–99.
[156] Roscoe R. The viscosity of suspensions of rigid spheres. Br J Appl Phys 1952;3 (8):267–9.
[157] Brinkman HC. The viscosity of concentrated suspensions and solutions. J Chem Phys 1952;20(4):571.
[158] Bakopoulos A. Fluid dynamics and mixing in three-phase coal and oil residue hydrogenation sieve cascade reactors. Chem Eng Sci 2001;56(17):5131–45.
[159] Thomas DG. Transport characteristics of suspension: VIII. a note on the viscosity of Newtonian suspensions of uniform spherical particles. J Colloid Sci 1965;20(3):267–77.
[160] Ford TF. Viscosity-concentration and fluidity-concentration relationships for suspensions of spherical particles in Newtonian liquids. J Phys Chem 1960;64 (9):1168–74.
[161] Eilers H. The viscosity of the emulsion of highly viscous substances as function of concentration. Kolloid-Zeitschrift 1941;97(3):313–21. German.
[162] Chong JS, Christiansen EB, Baer AD. Rheology of concentrated suspensions. J Appl Polym Sci 1971;15(8):2007–21.
[163] Fedors RF. Relationships between viscosity and concentration for Newtonian suspensions. J Colloid Interface Sci 1974;46(3):545–7.
[164] Frankel NA, Acrivos A. On the viscosity of a concentrated suspension of solid spheres. Chem Eng Sci 1967;22(6):847–53.
[165] Quemada D. Rheology of concentrated disperse systems and minimum energy dissipation principle. I. Viscosity–concentration relationship. Rheol Acta 1977;16(1):82–94.
[166] Mooney M. The viscosity of a concentrated suspension of spherical particles. J Colloid Sci 1951;6(2):162–70.
[167] Kawase Y, Ulbrecht JJ. Rheological properties of suspensions of solid spheres in non-Newtonian fluids. Chem Eng Commun 1983;20(3–4):127–36.
[168] Krieger IM, Dougherty TJ. A mechanism for non-Newtonian flow in suspensions of rigid spheres. Trans Soc Rheol 1959;3(1):137–52.
[169] Sengun MZ, Probstein RF. High-shear-limit viscosity and the maximum packing fraction in concentrated monomodal suspensions. Physicochem Hydrodyn 1989;11(2):229–41.
[170] Rabha S, Schubert M, Hampel U. Hydrodynamic studies in slurry bubble columns: experimental and numerical study. Chem Ing Tech 2013;85 (7):1092–8.
[171] Chilekar VP, Warnier MJF, Van der Schaaf J, Kuster BFM, Schouten JC, Van Ommen JR. Bubble size estimation in slurry bubble columns from pressure fluctuations. AIChE J 2005;51(7):1924–37.
[172] Luo XK, Lee DJ, Lau R, Yang GQ, Fan LS. Maximum stable bubble size and gas holdup in high-pressure slurry bubble columns. AIChE J 1999;45(4):665–80.
[173] Vandu CO, Koop K, Krishna R. Large bubble sizes and rise velocities in a bubble column slurry reactor. Chem Eng Technol 2004;27(11):1195–9.
[174] Kelkar BG, Shah YT, Carr NL. Hydrodynamics and axial mixing in a three-phase bubble column. Effects of slurry properties. Ind Eng Chem Process Des Dev 1984;23(2):308–13.
[175] Sada E, Kumazawa H, Lee CH. Influences of suspended fine particles on gas holdup and mass transfer characteristics in a slurry bubble column. AIChE J 1986;32(5):853–6.
[176] Jamialahmadi M, Müller-Steinhagen H. Effect of solid particles on gas hold-up in bubble columns. Can J Chem Eng 1991;69(1):390–3.
[177] Mena PC, Ruzicka MC, Rocha FA, Teixeira JA, Drahoš J. Effect of solids on homogeneous–heterogeneous flow regime transition in bubble columns. Chem Eng Sci 2005;60(22):6013–26.
[178] Milivojevic M, Pavlou S, Bugarski B. Liquid velocity in a high-solids-loading three-phase external-loop airlift reactor. J Chem Technol Biotechnol 2012;87 (11):1529–40.
[179] Murray P, Fan LS. Axial solids distribution in slurry bubble columns. Ind Eng Chem Res 1989;28(11):1697–703.
[180] Zhang K. Axial solid concentration distribution in tapered and cylindrical bubble columns. Chem Eng J 2002;86(3):299–307.
[181] Shaikh A, Al-Dahhan M. Scale-up of bubble column reactors: a review of current state-of-the-art. Ind Eng Chem Res 2013;52(24):8091–108.
[182] Onozaki M, Namiki Y, Ishibashi H, Kobayashi M, Itoh H, Hiraide M, et al. A process simulation of the NEDOL coal liquefaction process. Fuel Process Technol 2000;64(1–3):253–69.
[183] Jakobsen HA, Lindborg H, Dorao CA. Modeling of bubble column reactors: progress and limitations. Ind Eng Chem Res 2005;44(14):5107–51.
[184] Cao C, Dong S, Guo Q. Experimental and numerical simulation for gas–liquid phases flow structure in an external-loop airlift reactor. Ind Eng Chem Res 2007;46(22):7317–27.
[185] Joshi JB. Computational flow modelling and design of bubble column reactors. Chem Eng Sci 2001;56(21–22):5893–933.
[186] Zhang L, Huang Q. Research progress in the modeling theory of airlift loop reactor. Chin J Process Eng 2011;11(1):86–97.
[187] Tomiyama A. Drag, lift and virtual mass forces acting on a single bubble. In: Proceedings of the Third International Symposium on Two-Phase Flow Modeling and Experimentation; 2004 Sept 22–24; Pisa, Italy; 2004.
[188] Troshko AA, Hassan YA. A two-equation turbulence model of turbulent bubbly flows. Int J Multiph Flow 2001;27(11):1965–2000.
[189] Pfleger D, Becker S. Modelling and simulation of the dynamic flow behaviour in a bubble column. Chem Eng Sci 2001;56(4):1737–47.
[190] Zhang D, Deen NG, Kuipers JAM. Numerical simulation of the dynamic flow behavior in a bubble column: a study of closures for turbulence and interface forces. Chem Eng Sci 2006;61(23):7593–608.
[191] Huang Q, Yang C, Yu G, Mao ZS. CFD simulation of hydrodynamics and mass transfer in an internal airlift loop reactor using a steady two-fluid model. Chem Eng Sci 2010;65(20):5527–36.
[192] Huang Q, Yang C, Yu G, Mao ZS. Sensitivity study on modeling an internal airlift loop reactor using a steady 2D two-fluid model. Chem Eng Technol 2008;31(12):1790–8.
[193] Oey RS, Mudde RF, Portela LM, Van den Akker HEA. Simulation of a slurry airlift using a two-fluid model. Chem Eng Sci 2001;56(2):673–81.
[194] Wang TF, Wang JF, Jin Y. Experimental study and CFD simulation of hydrodynamic behaviours in an external loop airlift slurry reactor. Can J Chem Eng 2004;82(6):1183–90.
[195] Chen P, Duduković MP, Sanyal J. Three-dimensional simulation of bubble column flows with bubble coalescence and breakup. AIChE J 2005;51 (3):696–712.
[196] Chen P, Sanyal J, Duduković MP. Numerical simulation of bubble columns flows: effect of different breakup and coalescence closures. Chem Eng Sci 2005;60(4):1085–101.
[197] Frank T, Zwart PJ, Shi JM, Krepper E, Lucas D, Rohde U. Inhomogeneous MUSIG model—a population balance approach for polydispersed bubbly flows. In: Proceedings of International Conference for Nuclear Energy for New Europe; 2005 Sept 5–8; Bled, Slovenia; 2005.
[198] Yang N, Xiao Q. A mesoscale approach for population balance modeling of bubble size distribution in bubble column reactors. Chem Eng Sci 2017;170:241–50.

[199] Lehr F, Millies M, Mewes D. Bubble-size distributions and flow fields in bubble columns. AIChE J 2004;48(11):2426–43.
[200] Ni X, Jian H, Fitch AW. Computational fluid dynamic modelling of flow patterns in an oscillatory baffled column. Chem Eng Sci 2002;57(14):2849–62.
[201] Lestinsky P, Vecer M, Vayrynen P, Wichterle K. The effect of the draft tube geometry on mixing in a reactor with an internal circulation loop—a CFD simulation. Chem Eng Process 2015;94:29–34.
[202] Pan Y, Dudukovic MP, Chang M. Numerical investigation of gas-driven flow in 2-D bubble columns. AIChE J 2004;46(3):434–49.
[203] Luo H, Svendsen HF. Theoretical model for drop and bubble breakup in turbulent dispersions. AIChE J 1996;42(5):1225–33.
[204] Prince MJ, Blanch HW. Bubble coalescence and break-up in air-sparged bubble columns. AIChE J 1990;36(10):1485–99.
[205] Lo S. Application of MUSIG model to bubbly flows. AEA Technol 1996;230:8216–46.
[206] Bhole MR, Joshi JB, Ramkrishna D. CFD simulation of bubble columns incorporating population balance modeling. Chem Eng Sci 2008;63(8):2267–82.
[207] Pendyala VRR, Jacobs G, Luo M, Davis BH. Fischer–Tropsch synthesis: effect of start-up solvent in a slurry reactor. Catal Lett 2013;143(5):395–400.
[208] Sehabiague L, Lemoine R, Behkish A, Heintz YJ, Sanoja M, Oukaci R, et al. Modeling and optimization of a large-scale slurry bubble column reactor for producing 10,000 bbl/day of Fischer–Tropsch liquid hydrocarbons. J Chin Inst Chem Eng 2008;39(2):169–79.
[209] Choi KH, Chisti Y, Moo-Young M. Comparative evaluation of hydrodynamic and gas–liquid mass transfer characteristics in bubble column and airlift slurry reactors. Chem Eng J Biochem Eng J 1996;62(3):223–9.
[210] Lu X, Ding J, Wang Y, Shi J. Comparison of the hydrodynamics and mass transfer characteristics of a modified square airlift reactor with common airlift reactors. Chem Eng Sci 2000;55(12):2257–63.
[211] Ren X, Fang D, Jin J, Gao J. Study on flow patterns in different types of direct coal liquefaction reactors. Asia-Pac J Chem Eng 2009;4(5):563–7.
[212] Han T, Liu H, Xiao H, Chen A, Huang Q. Experimental study of the effects of apex section internals and conical section length on the performance of solid–liquid hydrocyclone. Chem Eng Res Des 2019;145:12–8.
[213] Dudukovic MP. Reaction engineering: status and future challenges. Chem Eng Sci 2010;65(1):3–11.